

**Nuclear Astrophysics**  
**SISSA, Fall 2006**

**The Structure of Compact Stars**

Omar Benhar

INFN and Department of Physics

Università "La Sapienza". I-00185 Roma, Italy



# Contents

<b>1</b>	<b>Equilibrium of compact stars</b>	<b>1</b>
1.1	Introduction . . . . .	1
1.2	Energy-density and pressure of the degenerate Fermi gas . . . . .	5
1.3	Dynamical content of the equation of state . . . . .	10
1.4	EOS of the degenerate Fermi gas . . . . .	12
1.5	Hydrostatic equilibrium and structure of white dwarfs . . . . .	13
1.6	Equilibrium equation in general relativity . . . . .	17
<b>2</b>	<b>Nuclear matter in the neutron star crust</b>	<b>21</b>
2.1	Overview of neutron star structure . . . . .	21
2.2	Outer crust . . . . .	24
2.2.1	Inverse $\beta$ -decay . . . . .	25
2.2.2	Neutronization . . . . .	29
2.3	Inner crust . . . . .	35
<b>3</b>	<b>Nuclear matter Matter in the the neutron star interior</b>	<b>39</b>
3.1	Nuclear matter at supranuclear desities . . . . .	39
3.2	Constraints on the nuclear matter EOS . . . . .	40
3.3	The nucleon-nucleon interaction . . . . .	44
3.4	The two-nucleon system . . . . .	46

3.5	Nonrelativistic many-body theory . . . . .	51
3.5.1	The few-nucleon systems . . . . .	52
3.5.2	Nuclear matter . . . . .	57
3.6	Relativistic mean field theory . . . . .	64

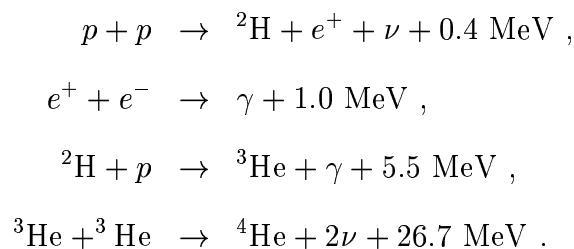
# Chapter 1

## Equilibrium of compact stars

### 1.1 Introduction

Compact stars, i.e. white dwarfs, neutron stars and black holes, are the final stage of stellar evolution. They are different from normal stars, whose stability against gravitational collapse is due to thermal pressure. In compact stars, the nuclear fuel necessary to ignite fusion reactions leading to heat production is no longer available, and the pressure needed for hydrostatic equilibrium is produced by different mechanisms, driven by quantum mechanical effects or interactions between the constituents of matter in the star interior.

The formation of a star is believed to be triggered by the contraction of a self-gravitating hydrogen cloud. As the density increases, the temperature also increases, and eventually becomes high enough to ignite the nuclear reactions turning hydrogen into helium:



Note that the above reactions are all exothermic, and energy is released in form of kinetic energy of the produced particles ( $1 \text{ MeV} = 1.6021917 \times 10^{-6} \text{ erg}$ ). Equilibrium is reached as soon as gravitational attraction is balanced by matter pressure.

When the nuclear fuel is exhausted the core stops producing heat, the internal pressure cannot be sustained and the contraction produced by gravitational attraction resumes. If the mass of the helium core is large enough its contraction, associated with a further increase of the temperature, can then lead to the ignition of new fusion reactions, resulting in the appearance of heavier nuclei: carbon and oxygen. Depending on the mass of the star, this process can take place several times, the final result being the formation of a core made of the most stable nuclear species, nickel and iron, at density  $\sim 10^{14} \text{ g/cm}^3$  (note that the central density of atomic nuclei is  $\rho_0 \approx 2 \times 10^{14} \text{ g/cm}^3$ ). The stages of nucleosynthesis for a star of mass  $\sim 25 M_\odot$  are summarized in Table 1.1. Even larger densities are believed to occur in the interior of neutron stars, astrophysical objects resulting from the contraction of the iron core in very massive stars ( $M > 4 M_\odot$ ).

Nuclear fuel	Main products	Temperature [°K]	Density [g/cm <sup>3</sup> ]	Duration [yrs]
H	He	$6 \times 10^7$	5	$7 \times 10^6$
He	C, O	$2 \times 10^8$	700	$5 \times 10^5$
C	O, Ne, Mg	$9 \times 10^8$	$2 \times 10^5$	600
Ne	O, Mg, Si	$1.7 \times 10^9$	$4 \times 10^5$	1
O	Si, S	$2.3 \times 10^9$	$10^7$	0.5
Si	Fe	$4 \times 10^9$	$3 \times 10^7$	0.0025

Table 1.1: Stages of nucleosynthesis for a star of mass  $\sim 25 M_\odot$

If the star is sufficiently small, so that the gravitational contraction of the core does

not produce a temperature high enough to ignite the burning of heavy nuclei, it will eventually turn into a white dwarf, i.e. a star consisting mainly of helium, carbon and oxygen.

The existence of white dwarfs was predicted in 1844 by the astronomer Friederich Bessel, who noticed that Sirius, a very bright star close to the earth, exhibited an orbital motion around a point in space that was apparently empty, as if it were part of a binary system with another star not yet observed. The mysterious partner, optically resolved by Alvan Clark in 1863, was given the name Sirius B.

The mass of Sirius B, determined from Kepler's third law, is  $\sim 1 M_{\odot}$  ( $M_{\odot} = 1.989 \times 10^{33}$  g denotes the mass of the sun), while its radius, obtained combining the observed luminosity and the distance from the earth, is  $\sim 5 \times 10^3$  km, much less than the solar radius ( $R_{\odot} \sim 7 \times 10^5$  km). In his book *The Internal Constitution of the Stars*, published in 1926, the astronomer Sir Arthur Eddington wrote the famous sentence "we have a star of mass about equal to the sun and radius much less than Uranus".

The over 2000 observed white dwarfs have luminosity  $L \sim 10^{-2} L_{\odot}$  ( $L_{\odot} = 4 \times 10^{33}$  erg s $^{-1}$ ) and surface temperature  $T_s \sim 10^4$  °K. The radius of many white dwarfs has been determined from their measured flux, defined as

$$F(D) = \frac{L}{4\pi D^2}, \quad (1.1)$$

where  $D$  is the distance from the earth, obtained using the parallax method. Combining the above equation to the equation describing black body emission

$$L = 4\pi\sigma R^2 T_s^4, \quad (1.2)$$

one obtains

$$R = \sqrt{\frac{F D^2}{\sigma T_s^4}}. \quad (1.3)$$

The measured values of mass and radius of three white dwarfs are given in Table 1.2.

The corresponding average densities are  $\sim 10^7$  g/cm<sup>3</sup>, to be compared to the the typical density of terrestrial macroscopic objects, not exceeding  $\sim 20$  g/cm<sup>3</sup>.

	Mass [ $M_{\odot}$ ]	Radius [ $R_{\odot}$ ]
Sirius B	$1.000 \pm 0.016$	$0.0084 \pm 0.0002$
Procyon B	$0.604 \pm 0.018$	$0.0096 \pm 0.0004$
40 Eri B	$0.501 \pm 0.011$	$0.0136 \pm 0.0002$

Table 1.2: Measured mass and radius of three white dwarfs

While the structure of terrestrial matter is mainly dictated by electromagnetic interactions, at much higher density the picture changes dramatically. The role of electromagnetic interactions is negligible and quantum mechanical effects and nuclear interactions become important. The effort to understand the structure of the white dwarfs triggered the first studies of physics of dense matter. More recently, these investigations have been considerably extended, to describe the physical properties of different types of dense matter of astrophysical and cosmological interest.

Of particular relevance is the understanding of the structure of matter in the interior of neutron stars, whose existence was predicted right after the discovery of the neutron. There are two very important differences between neutron stars and white dwarfs: i) due to the large densities involved, up to  $\sim 10^{15}$  g/cm<sup>3</sup>, neutron star properties are strongly affected by relativistic effects, and ii) the dynamics of strong interactions between the constituents of matter in the star interior plays a crucial role in determining the equilibrium. The physics of neutron star matter will be discussed in Chapters 2 and 3

As a pedagogical example, in Sections 1.2-1.5 we will first discuss in detail white



dwarfs, whose stability is due to the pressure of a degenerate electron gas.

## 1.2 Energy-density and pressure of the degenerate Fermi gas

Let us consider a system of noninteracting electrons uniformly distributed in a cubic box of volume  $V = L^3$ . If the temperature is sufficiently low, so that thermal energies can be neglected, the lowest quantum levels are occupied by two electrons, one for each spin state. Both electrons have the same energy, i.e. they are *degenerate*. This configuration corresponds to the ground state of the system. A gas of noninteracting electrons in its ground state is said to be *fully degenerate*. At higher temperature, the thermal energy can excite electrons to higher energy states, leaving some of the lower lying levels not fully degenerate.

As the electrons are uniformly distributed, their wave functions exhibit translational invariance. They are eigenfunctions of the generator of spacial translation, i.e. the momentum operator, i.e. plane waves of the form

$$\phi_{\mathbf{p}}(\mathbf{r}) = \sqrt{\frac{1}{V}} e^{i\mathbf{p}\cdot\mathbf{r}} , \quad (1.4)$$

satisfying periodic boundary conditions ( $x$ ,  $y$  and  $z$  denote the components of the vector  $\mathbf{r}$ , specifying the electron position)

$$\phi_{\mathbf{p}}(x, y, z) = \phi_{\mathbf{p}}(x + n_x L, y + n_y L, z + n_z L) , \quad (1.5)$$

with  $n_x, n_y, n_z = 0, \pm 1, \pm 2, \dots$ . The above equation obviously implies the relations ( $\mathbf{p} \equiv (p_x, p_y, p_z)$ )

$$p_x = \frac{2\pi n_x}{L}, \quad p_y = \frac{2\pi n_y}{L}, \quad p_z = \frac{2\pi n_z}{L} , \quad (1.6)$$

which in turn determine the momentum eigenvalues.

Each quantum state is associated with an eigenvalue of the momentum  $\mathbf{p}$ , i.e. with a specific triplet of integers  $(n_x, n_y, n_z)$ . The corresponding energy eigenvalue is ( $p^2 = |\mathbf{p}|^2 = p_x^2 + p_y^2 + p_z^2$ )

$$\epsilon_p = \frac{p^2}{2m_e} = \left(\frac{2\pi}{L}\right)^2 \frac{1}{2m_e} (n_x^2 + n_y^2 + n_z^2), \quad (1.7)$$

$m_e$  being the electron mass ( $m_e = 9.11 \times 10^{-28}$  g or 0.511 MeV). The highest energy reached, called the Fermi energy of the system, is denoted by  $\epsilon_F$ , and the associated momentum, the Fermi momentum, is  $p_F = \sqrt{2m_e\epsilon_F}$ .

The number of quantum states with energy less or equal to  $\epsilon_F$  can be easily calculated. Since each triplet  $(n_x, n_y, n_z)$  corresponds to a point in a cubic lattice with unit lattice spacing, the number of momentum eigenstates is equal to the number of lattice points within a sphere of radius  $R = p_FL/(2\pi)$ . The number of electrons in the system can then be obtained from (note: the factor 2 takes into account spin degeneracy, i.e. the fact that there are two electrons with opposite spin projections sitting in each momentum eigenstate)

$$N = 2 \frac{4\pi}{3} R^3 = V \frac{p_F^3}{3\pi^2}, \quad (1.8)$$

and the electron number density, i.e. the number of electrons per unit volume, is given by

$$n_e = \frac{N}{V} = \frac{p_F^3}{3\pi^2}. \quad (1.9)$$

The total ground state energy can be easily evaluated from

$$E = 2 \sum_{p < p_F} \frac{p^2}{2m_e} \quad (1.10)$$

replacing (use (1.6) again and take the limit of large  $L$ , corresponding to vanishingly small level spacing)

$$\sum_{p < p_F} \rightarrow \frac{V}{(2\pi^3)} \int_{p < p_F} d^3p \quad (1.11)$$

to obtain

$$E = 2 \frac{V}{(2\pi^3)} 4\pi \int_0^{p_F} p^2 dp \frac{p^2}{2m_e} . \quad (1.12)$$

The resulting energy density is

$$\epsilon = \frac{E}{V} = \frac{1}{(2\pi)^3} 4\pi \frac{p_F^5}{5m_e} . \quad (1.13)$$

From Eq.(1.9) it follows that the Fermi energy can be written in terms of the number density according to

$$\epsilon_F = \frac{p_F^2}{2m_e} = \frac{1}{2m_e} (3\pi^2 n_e)^{2/3} . \quad (1.14)$$

The above equation can be used to define a density  $n_0$  such that for  $n_e \gg n_0$  the electron gas at given temperature  $T$  is fully degenerate. Full degeneracy is realized when the thermal energy  $K_B T$  ( $K_B$  is the Boltzman constant:  $K_B = 1.38 \times 10^{-16}$  erg/°K) is much smaller than the Fermi energy  $\epsilon_F$ , i.e. when

$$n_e \gg n_0 = \frac{1}{3\pi^2} (2m_e K_B T)^{3/2} . \quad (1.15)$$

For an ordinary star at the stage of hydrogen burning, like the Sun, the interior temperature is  $\sim 10^7$  °K, and the corresponding value of  $n_0$  is  $\sim 10^{26}$  cm<sup>-3</sup>. If we assume that the electrons come from a fully ionized hydrogen gas, the *matter* density of the proton-electron plasma is

$$\rho = (m_p + m_e) n_0 \sim 200 \text{ g/cm}^3 , \quad (1.16)$$

$m_p$  being the proton mass ( $m_p = 1.67 \times 10^{-24}$  g). This density is high for most stars in the early stage of hydrogen burning, while for ageing stars that have developed a substantial helium core the density ( $m_n$  denotes the neutron mass:  $m_n \approx m_p$ ).

$$\rho = (m_p + m_n + m_e) n_0 \sim 400 \text{ g/cm}^3 \quad (1.17)$$

can be largely exceeded within the core. For example, white dwarfs have core densities of the order of  $10^7 \text{ g/cm}^3$ . As a consequence, in the study of their structure thermal energies can be safely neglected, the primary role being played by the degeneracy energy  $p^2/2m_e$ .

The pressure  $P$  of the electron gas, i.e. the force per unit area on the walls of the box, is defined in kinetic theory as the rate of momentum transferred by the electrons colliding on a surface of unit area. The pressure generated on the wall of the box lying on the  $yz$  plane by electrons moving with momentum  $p_x$  and velocity  $v_x$  parallel to the  $x$  axis is

$$P(p_x) = \frac{1}{L^2} \frac{dp_x}{dt} = \frac{1}{L^2} (2p_x) \left( \frac{1}{2} n_e v_x L^2 \right) = \frac{N}{V} p_x v_x . \quad (1.18)$$

In the above equation, the first terms in round brackets is the momentum transfer associated with the reflection of one electron off the box wall, while the second term is the electron flux, i.e. the number of electrons hitting the wall during the time  $dt$ . The factor  $1/2$  accounts for the fact that half of the electrons go the wrong way and do not collide with the box wall. Since the system is isotropic

$$p_x v_x = \frac{1}{3} (p_x v_x + p_y v_y + p_z v_z) = \frac{1}{3} (\mathbf{p} \cdot \mathbf{v}) = \frac{1}{3} (pv) , \quad (1.19)$$

and the total pressure can be obtained from (use  $v = (\partial \epsilon_p / \partial p) = p/m_e$ )

$$P = 2 \frac{1}{N} \sum_{p < p_F} \frac{N}{V} \frac{1}{3} (pv) = \frac{2}{3} \frac{1}{(2\pi)^3} 4\pi \int_0^{p_F} p^2 dp (pv) = \frac{1}{(2\pi)^3} 4\pi \frac{2p_F^5}{15m_e} . \quad (1.20)$$

Note that the above result can also be obtained from the standard thermodynamical definition of pressure

$$P = - \left( \frac{\partial E}{\partial V} \right)_N , \quad (1.21)$$

using  $E$  given by Eq.(1.12) and  $(\partial p_F / \partial V)_N = -p_F / (3V)$ .

Eq.(1.20) shows that the pressure of a degenerate Fermi gas decreases linearly as the mass of the constituent particle increases. For example, the pressure of an electron gas at number density  $n_e$  is  $\sim 2000$  times larger than the pressure of a gas of protons at the same number density.

So far, we have been assuming that the electrons in the degenerate gas be nonrelativistic. However, the properties of the system depend primarily on the distribution of quantum states, which is dictated by translation invariance only, and is not affected by this assumption. Releasing the nonrelativistic approximation simply amounts to replace the nonrelativistic kinetic energy with its relativistic counterpart:

$$\frac{p^2}{2m_e} \rightarrow \sqrt{p^2 + m_e^2} - m_e . \quad (1.22)$$

The transition from the nonrelativistic regime to the relativistic one occurs when the electron energy becomes comparable to the energy associated with the electron rest mass,  $m_e$ . It is therefore possible to define a density  $n_c$  such that at  $n_e \ll n_c$  the system is nonrelativistic, while  $n_e \gg n_c$  corresponds to the relativistic regime. The value of  $n_c$  can be found requiring that the Fermi energy at  $n_e = n_c$  be equal to  $m_e$ . The resulting expression is

$$n_c = \frac{2^{3/2}}{3\pi^2} m_e^3 \sim 1.6 \times 10^{30} \text{cm}^{-3} . \quad (1.23)$$

The energy density of a fully degenerate gas of relativistic electrons can be obtained from (compare to Eqs.(1.12) and (1.13))

$$\epsilon = 2 \frac{1}{(2\pi^3)} 4\pi \int_0^{p_F} p^2 dp \left[ \sqrt{p^2 + m_e^2} - m_e \right] , \quad (1.24)$$

while the equation for the pressure reads (compare to Eq.(1.20) and use again  $v = \partial\epsilon_p/\partial p$  with the relativistic  $\epsilon_p$ )

$$P = \frac{2}{3} \frac{1}{(2\pi)^3} 4\pi \int_0^{p_F} p^2 dp \left( p \frac{\partial\epsilon_p}{\partial p} \right) . \quad (1.25)$$

Carrying out the integrations involved in Eqs.(1.24) and (1.25) we find:

$$\epsilon = \frac{\pi m_e}{\lambda_e^3} \left[ t (2t^2 + 1) \sqrt{t^2 + 1} - \ln \left( t + \sqrt{t^2 + 1} \right) \right] \quad (1.26)$$

and

$$P = \frac{\pi m_e}{\lambda_e^3} \left[ \frac{1}{3} t (2t^2 + 1) \sqrt{t^2 + 1} + \ln \left( t + \sqrt{t^2 + 1} \right) \right] , \quad (1.27)$$

where  $\lambda_e = 2\pi/m_e c$  is the electron Compton wavelength and (see Eq.(1.14))

$$t = \frac{p_F}{m_e} = \frac{1}{m_e} (3\pi^2 n_e)^{1/3} \quad (1.28)$$

Eqs.(1.26) and (1.27) give the energy density and pressure of a fully degenerate electron gas as a function of the variable  $t$ , which can in turn be written in terms of the number density  $n_e$  according to Eq.(1.28).

As a final remark, we briefly discuss the possible relevance of electrostatic interactions. In a fully ionized plasma their effect can be estimated noting that the corresponding energy is

$$E_c = Z \frac{e^2}{\langle r \rangle} \propto Z e^2 n_e^{1/3} , \quad (1.29)$$

where  $Ze$  is the electric charge of the ions and  $\langle r \rangle \propto n_e^{1/3}$  is the typical electron-ion separation distance. It follows that the ratio between  $E_c$  and the Fermi energy is given by

$$\frac{E_c}{\epsilon_F} \propto \frac{1}{n_e^{1/3}} . \quad (1.30)$$

As a consequence, for sufficiently high density the contribution of electrostatic interactions becomes negligibly small. As this condition is largely satisfied at the densities typical of white dwarfs, electrons can be safely described as a fully degenerate Fermi gas.

### 1.3 Dynamical content of the equation of state

The equation of state (EOS) is a nontrivial relation linking the thermodynamic variables specifying the state of a physical system. The best known example of EOS is Boyle's *ideal gas law*, stating that the pressure of a collection of  $N$  noninteracting, pointlike classical particles, enclosed in a volume  $V$ , grows linearly with the temperature  $T$  and the average particle density  $n = N/V$ .

The ideal gas law provides a good description of very dilute systems. In general, the EOS can be written as an expansion of the pressure,  $P$ , in powers of the density (in this

Section we use units such that  $K_B = 1$ ):

$$P = nT [1 + nB(T) + n^2C(T) + \dots] . \quad (1.31)$$

The coefficients appearing in the above series, that goes under the name of *virial expansion*, are functions of temperature only. They describe the deviations from the ideal gas law and can be calculated in terms of the underlying elementary interaction. Therefore, the EOS carries a great deal of dynamical information, and its knowledge makes it possible to establish a link between measurable *macroscopic* quantities, such as pressure or temperature, and the forces acting between the constituents of the system at *microscopic* level.

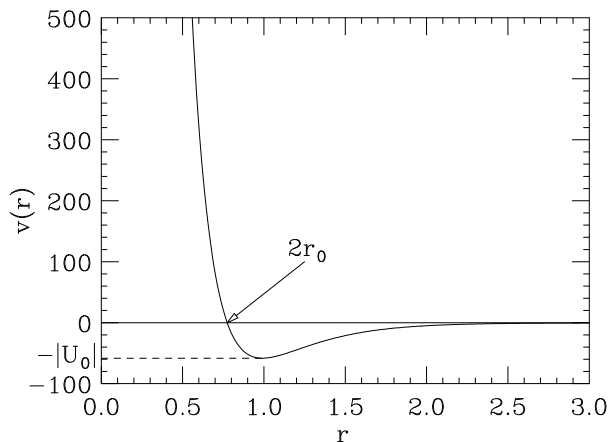


Figure 1.1: Behavior of the potential describing the interactions between constituents of a van der Waals fluid (the interparticle distance  $r$  and  $v(r)$  are both given in arbitrary units).

This point is best illustrated by the van der Waals EOS, which describes a collection of particles interacting through a potential featuring a strong repulsive core followed by a weaker attractive tail (see Fig.1.1). At  $|U_0|/T \ll 1$ ,  $U_0$  being the strength of the attractive part of the potential, the van der Waals EOS can be cast in the simple form

$$P = \frac{nT}{1 - nb} - an^2 , \quad (1.32)$$

and the two quantities  $a$  and  $b$ , taking into account interaction effects, can be directly related to the potential  $v(r)$  through

$$a = 2\pi \int_{2r_0}^{\infty} |v(r)|^2 r^2 dr \quad , \quad b = \frac{16}{3} \pi r_0^3 \quad , \quad (1.33)$$

where  $2r_0$  denotes the radius of the repulsive core (see Fig.1.1).

In spite of its simplicity, the van der Waals EOS describes most of the features of both the gas and liquid phases of the system, as well as the nature of the phase transition.

## 1.4 EOS of the degenerate Fermi gas

Equation (1.27) is the EOS of the degenerate electron gas, providing a link between its pressure  $P$  and the matter density  $\rho$ , which is in turn related to the electron number density  $n_e$  through

$$\rho = \frac{m_p}{Y_e} n_e \quad , \quad (1.34)$$

where  $Y_e$  is the number of electrons per nucleon in the system. For example, for a fully ionized helium plasma  $Y_e = 0.5$ , whereas for a plasma of iron nuclei  $Y_e = Z/A = 26/56 = 0.464$  ( $Z$  and  $A$  denote the nuclear charge and mass number, respectively).

The EOS of the fully degenerate electron gas takes a particularly simple form in the nonrelativistic limit (corresponding to  $t \ll 1$ ), as well as in the extreme relativistic limit (corresponding to  $t \gg 1$ ). From Eq.(1.27) we find

$$P = \frac{8}{15} \frac{\pi m_e}{\lambda_e^3} \left( \frac{3\pi^2 Y_e}{m_p} \right)^{5/3} \rho^{5/3} \quad (1.35)$$

for  $e_F \ll m_e$  and

$$P = \frac{2}{3} \frac{\pi m_e}{\lambda_e^3} \left( \frac{3\pi^2 Y_e}{m_p} \right)^{4/3} \rho^{4/3} \quad (1.36)$$

for  $e_F \gg m_e$ .

A EOS that can be written in the form

$$P \propto \rho^\Gamma \quad , \quad (1.37)$$



is said to be *polytropic*. The exponent  $\Gamma$  is called *adiabatic index*, whereas the quantity  $n$ , defined through

$$\Gamma = 1 + \frac{1}{n}, \quad (1.38)$$

goes under the name of *polytropic index*.

The adiabatic index, whose definition for a generic equation of state reads

$$\Gamma = \frac{d(\ln P)}{d(\ln \rho)}. \quad (1.39)$$

is related to the compressibility  $\chi$ , characterizing the change of pressure with volume according to

$$\frac{1}{\chi} = -V \left( \frac{\partial P}{\partial V} \right)_N = \rho \left( \frac{\partial P}{\partial \rho} \right)_N \quad (1.40)$$

through

$$\Gamma = \frac{1}{\chi P}. \quad (1.41)$$

The compressibility is also simply related to speed of sound in matter,  $c_s$ , defined as

$$c_s = \left( \frac{\partial P}{\partial \rho} \right)^{1/2} = \frac{1}{\chi \rho}. \quad (1.42)$$

The magnitude of the adiabatic index reflects the so called *stiffness* of the equation of state. Larger stiffness corresponds to more incompressible matter. As we will see in the following Chapters, stiffness turns out to be critical in determining a number of stellar properties.

## 1.5 Hydrostatic equilibrium and structure of white dwarfs

Let us assume that white dwarfs consist of a plasma of fully ionized helium at zero temperature. The pressure of the system,  $P$ , is provided by the electrons, the contribution of the helium nuclei being negligible due to their large mass. For any given value of the matter density  $\rho$ ,  $P$  can be computed from Eqs.(1.27) and (1.28) (in this case  $Y_e = 0.5$ ,

implying  $n_e = \rho/2m_p$ ). The results of this calculation are shown by the diamonds in fig. 1.2. For comparison, the nonrelativistic (Eq.(1.35)) and extreme relativistic (Eq.(1.36)) limits are also shown by the solid and dashed line, respectively. Note that the value of matter density corresponding to  $n_c$  defined in Eq.(1.23) is  $\rho \sim 6.3 \cdot 10^6 \text{ g/cm}^3$ .

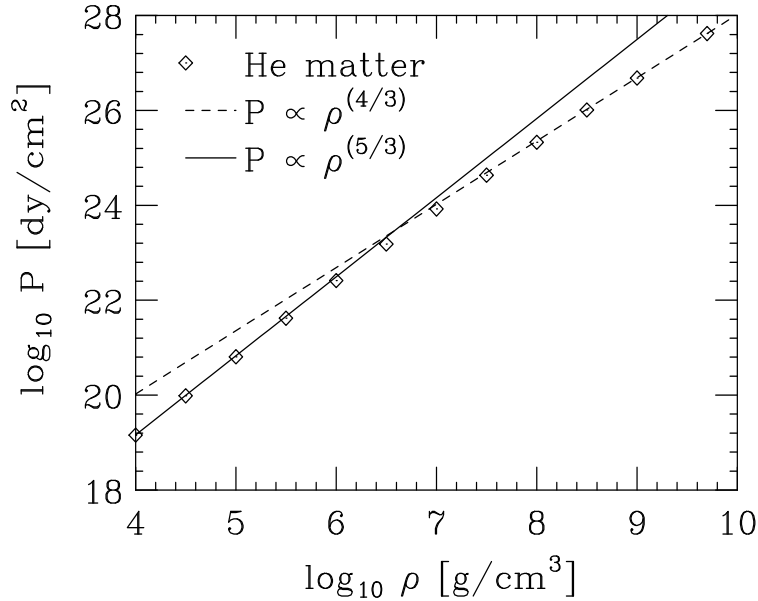


Figure 1.2: Equation of state of a fully ionized helium plasma at zero temperature (diamonds). The solid and dashed line correspond to the nonrelativistic and extreme relativistic limits, respectively.

In order to show the sensitivity of the EOS to the value of  $Y_e$ , in Fig. 1.3 the EOS of the fully ionized helium plasma ( $Y_e = 0.5$ ) is compared to that of a hydrogen plasma ( $Y_e = 1$ ).

The surface gravity of white dwarfs,  $GM/R$  ( $G$  is the gravitational constant), is small, of order  $\sim 10^{-4}$ . Hence, their structure can be studied assuming that they consist of a spherically symmetric fluid in hydrostatic equilibrium and neglecting relativistic effects.

Consider a perfect fluid in thermodynamic equilibrium, subject to gravity only. The

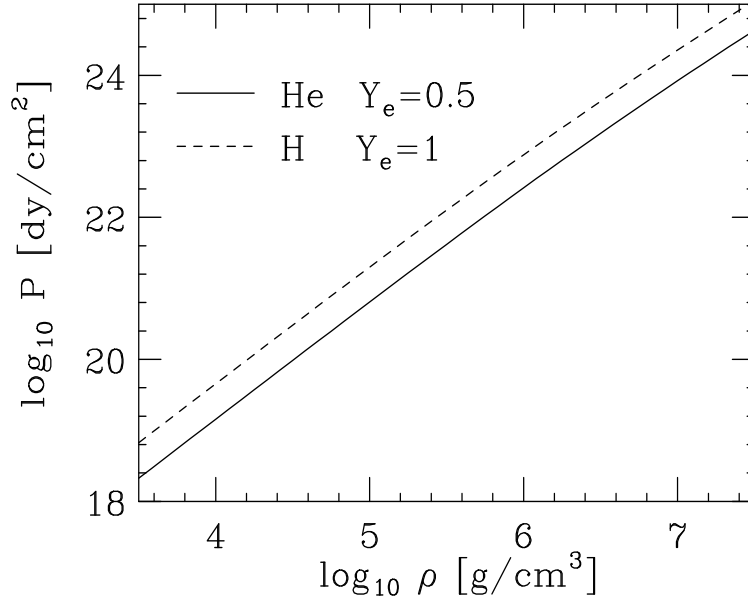


Figure 1.3: Comparison between the EOS of a fully ionized plasma of helium (solid line) and hydrogen (dashed line).

Euler equation corresponding to mechanical equilibrium reads

$$\nabla P = -\rho (\nabla \phi) , \quad (1.43)$$

where  $\rho$  is the density and the gravitational potential  $\phi$  satisfies Poisson's equation

$$\nabla^2 \phi = 4\pi G \rho . \quad (1.44)$$

Acting on both sides of Eq.(1.43) with the operator  $\nabla$  and using Eq.(1.44) we find the relation

$$\nabla \left( \frac{1}{\rho} \nabla P \right) = -\nabla^2 \phi = -4\pi G \rho , \quad (1.45)$$

which, in the case of a spherically symmetric fluid becomes

$$\frac{1}{r^2} \frac{d}{dr} \left( r^2 \frac{dP}{dr} \right) = -4\pi G \rho . \quad (1.46)$$

Finally, Eq.(1.46) can be rewritten in the form

$$\frac{dP}{dr} = -\rho(r) \frac{GM(r)}{r^2} , \quad (1.47)$$

with  $M(r)$  given by

$$M(r) = 4\pi \int_0^r \rho(r') r'^2 dr' . \quad (1.48)$$

The above equations simply state the well known result that, at equilibrium, the gravitational force acting on an volume element at distance  $r$  from the center of the star is balanced by the force produced by the space variation of the pressure.

Given a EOS, Eq.(1.47) can be integrated numerically for any value of the central density  $\rho_c$  to obtain the radius of the star, i.e. the value of  $r$  corresponding to vanishingly small density. The mass can then be obtained from eq.(1.48).

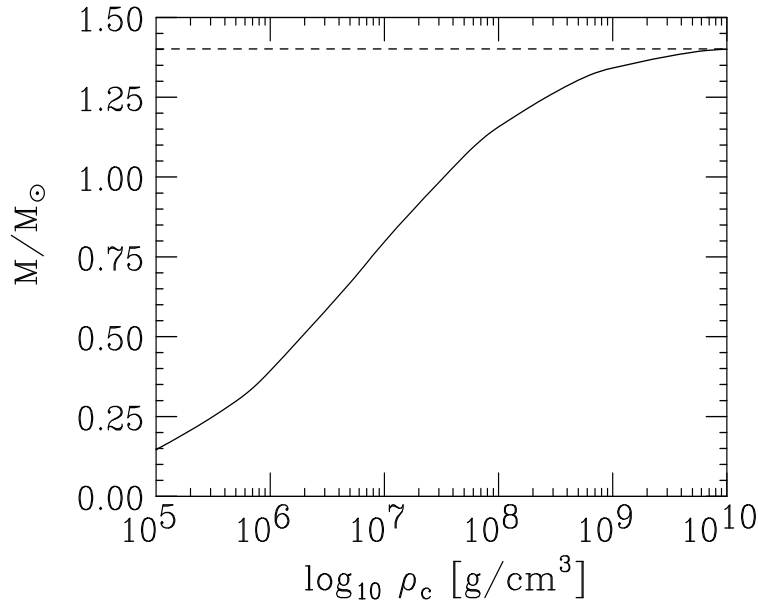


Figure 1.4: Dependence of the mass of a white dwarf upon its central density, obtained from the integration of eq.(1.47) using the equation of state of a fully ionized helium plasma.

For polytropic EOS Eqs.(1.47) and (1.48) reduce to the Lane-Emden equation, whose integration with the polytropic index  $n = 3/2$ , corresponding to the non relativistic regime, yields the relation

$$M = \frac{2.79}{Y_e^2} \left( \frac{\rho_c}{\bar{\rho}} \right)^{1/2} M_\odot , \quad (1.49)$$

where  $\bar{\rho}$  denotes the value of matter density corresponding to the electron number density of Eq.(1.23). The resulting values of  $M$  agree with the results of astronomical observations of white dwarfs. It is very important to realize, however, that Lane-Emden equation predicts the existence of equilibrium configurations for any values of the star mass.

In 1931 Chandrasekhar pointed out that, due to the large Fermi energies, the non relativistic treatment of the electron gas was not justified. Replacing the EOS of Eq.(1.35) with its relativistic counterpart, Eq.(1.36), he predicted the existence of a maximum mass for white dwarfs. If the mass exceeds this limiting value gravitational attraction prevails on the pressure gradient, and the star becomes unstable against gravitational collapse.

The dependence of the mass of a white dwarf upon its central density, obtained from integration of Eq.(1.47) using the equation of state of a fully ionized helium plasma, is illustrated in Fig.1.4. The figure shows that the mass increases as the central density increases, until a value  $M \sim 1.44 M_{\odot}$  is reached at  $\rho_0 \sim 10^{10} \text{ g/cm}^3$ . This value is close to that found by Chandrasekhar. However, as we will see in the following Chapters, at  $\rho \sim 10^8 \text{ g/cm}^3$  the *neutronization* process sets in, and the validity of the description in terms of a helium plasma breaks down. At  $\rho \geq 10^8 \text{ g/cm}^3$ , matter does not support pressure as effectively as predicted by the equation of state of the helium plasma. As a consequence, a more realistic estimate of the limiting mass, generally referred to as the *Chandrasekhar mass*, is given by the mass corresponding to a central density of  $10^8 \text{ g/cm}^3$ , i.e.  $\sim 1.2 M_{\odot}$ .

## 1.6 Equilibrium equation in general relativity

The Newtonian equilibrium equation employed in the case of white dwarfs represents a good approximation when the matter density does not produce an appreciable space-time curvature, in which case the metric is simply given by

$$ds^2 = \eta_{\mu\nu} dx^{\mu} dx^{\nu} \quad (1.50)$$

with

$$\eta = \begin{pmatrix} -1 & 0 & 0 & 0 \\ 0 & 1 & 0 & 0 \\ 0 & 0 & 1 & 0 \\ 0 & 0 & 0 & 1 \end{pmatrix} \quad (1.51)$$

In Einstein's theory of general relativity, Eq.(1.50) is replaced by

$$ds^2 = g_{\mu\nu} dx^\mu dx^\nu, \quad (1.52)$$

where the metric tensor  $g_{\mu\nu}$  is a function of space-time coordinates.

The effects of space-time distortion are negligible when the surface gravitational potential fulfills the requirement  $GM/R \ll 1$ . This condition is satisfied by white dwarfs, having  $GM/R \sim 10^{-4}$ , but not by neutron stars, whose larger density leads to much higher values of  $GM/R$ , typically  $\sim 10^{-1}$ .

Relativistic corrections to the hydrostatic equilibrium equations (1.47) and (1.48) are obtained solving Einstein's field equations

$$G_{\mu\nu} = 8\pi G T_{\mu\nu}, \quad (1.53)$$

where  $T_{\mu\nu}$  is the energy-momentum tensor, while the Einstein's tensor  $G_{\mu\nu}$  is defined in terms of the metric tensor  $g_{\mu\nu}$ . Equations (1.53) state the relation between the distribution of matter, described by  $T_{\mu\nu}$ , and space-time geometry, described by  $g_{\mu\nu}$ .

Consider a star consisting of a static and spherically symmetric distribution of matter in chemical, hydrostatic and thermodynamic equilibrium. The metric of the corresponding gravitational field can be written in the form ( $x^0 = t, x^1 = \varphi, x^2 = r, x^3 = \theta$ )

$$ds^2 = g_{\mu\nu} dx^\mu dx^\nu = e^{2\nu(r)} dt^2 - e^{2\lambda(r)} dr^2 - r^2(d\theta^2 + \sin^2 \theta d\varphi^2), \quad (1.54)$$

implying

$$g = \begin{pmatrix} e^{2\nu(r)} & 0 & 0 & 0 \\ 0 & -e^{2\lambda(r)} & 0 & 0 \\ 0 & 0 & -r^2 & 0 \\ 0 & 0 & 0 & -r^2 \sin^2 \theta \end{pmatrix}, \quad (1.55)$$

$\nu(r)$  e  $\lambda(r)$  being functions to be determined solving Einstein's equations

Under the standard assumption that matter in the star interior behave as an ideal fluid, the energy-momentum tensor can be written in the form

$$T_{\mu\nu} = (\epsilon + P)u_\mu u_\nu - P g_{\mu\nu} , \quad (1.56)$$

where  $\epsilon$  and  $P$  denote energy density and pressure, respectively, while

$$u_\mu = \frac{dx_\mu}{d\tau} \equiv (e^{-\nu(r)}, 0, 0, 0) \quad (1.57)$$

is the local four-velocity.

The Einstein tensor  $G_{\mu\nu}$ , given by

$$G_{\mu\nu} = R_{\mu\nu} - \frac{1}{2}g_{\mu\nu}R , \quad (1.58)$$

with

$$R = g^{\mu\nu} R_{\mu\nu} \quad (1.59)$$

depends on  $g_{\mu\nu}$  through the Christoffel symbols

$$\Gamma^\lambda_{\mu\nu} = \frac{1}{2}g^{\alpha\lambda}(g_{\alpha\mu,\nu} + g_{\alpha\nu,\mu} + g_{\mu\nu,\alpha}) , \quad (1.60)$$

appearing in the definition of the Ricci tensor  $R_{\mu\nu}$

$$R_{\mu\nu} = \Gamma^\alpha_{\mu\alpha,\nu} - \Gamma^\alpha_{\mu\nu,\alpha} - \Gamma^\alpha_{\mu\nu}\Gamma^\beta_{\alpha\beta} + \Gamma^\alpha_{\mu\beta}\Gamma^\beta_{\nu\alpha} . \quad (1.61)$$

From Eqs.(1.61) and (1.54) it follows that the nonvanishing elements of  $R_{\mu\nu}$  are

$$\begin{aligned} R_{00} &= \left[ -\nu'' + \lambda'\nu' - (\nu')^2 - \frac{2\nu'}{r} \right] e^{2(\nu-\lambda)} , \\ R_{11} &= \nu'' - \lambda'\nu' + (\nu')^2 - \frac{2\lambda'}{r} \\ R_{22} &= (1 + r\nu' - r\lambda') e^{-2\lambda} - 1 \\ R_{33} &= R_{22} \sin^2 \theta , \end{aligned} \quad (1.62)$$

implying

$$R = \left[ -2\nu'' + 2\lambda'\nu' - 2(\nu')^2 - \frac{2}{r^2} + \frac{4\lambda'}{r} - \frac{4\nu'}{r} \right] e^{-2\lambda} + \frac{2}{r^2} . \quad (1.63)$$

Substitution of Eqs.(1.56),(1.62) and (1.63) into Eqs.(1.53) leads to the system of differential equations

$$\begin{aligned} \left( \frac{1}{r^2} - \frac{2\lambda'}{r} \right) e^{-2\lambda} - \frac{1}{r^2} &= 8\pi G\epsilon(r) \\ \left( \frac{1}{r^2} + \frac{2\nu'}{r} \right) e^{-2\lambda} - \frac{1}{r^2} &= -8\pi GP(r) \\ \left[ \nu'' + (\nu')^2 - \lambda'\nu' + \frac{\nu' - \lambda'}{r} \right] e^{-2\lambda} &= -8\pi GP(r), \end{aligned}$$

where  $\epsilon(r)$  and  $P(r)$  denote the space distribution of energy density and pressure, respectively.

The above equations can be cast in the form originally derived by Tolman Oppenheimer and Volkoff (TOV)

$$\frac{dP(r)}{dr} = -\epsilon(r) \frac{GM(r)}{r^2} \left[ 1 + \frac{P(r)}{\epsilon(r)} \right] \left[ 1 + \frac{4\pi r^3 P(r)}{M(r)} \right] \left[ 1 - \frac{2GM(r)}{r} \right]^{-1} \quad (1.64)$$

with

$$\frac{dM(r)}{dr} = 4\pi r^2 \epsilon(r) . \quad (1.65)$$

The first term in the right hand side of Eq.(1.64) is the newtonian gravitational force. It is the same as the one appearing in Eq.(1.47), but with matter density replaced by energy density. The first two additional factors take into account relativistic corrections, that become vanishingly small in the limit  $p_F/m \rightarrow 0$ ,  $m$  and  $p_F$  being the mass and Fermi momentum of the star constituents, respectively. Finally, the third factor describes the effect of space-time curvature. Obviously, in the nonrelativistic limit all additional factors reduce to unity, and Eq.(1.64) reduces to the classical equilibrium equation (1.47).



# Chapter 2

## Nuclear matter in the neutron star crust

### 2.1 Overview of neutron star structure

The temperatures attained in stars whose initial mass is larger than  $\sim M_{\odot}$  are high enough to bring nucleosynthesis to its final stage (see Table 1.1), i.e. to the formation of a core of  ${}^{56}\text{Fe}$ . If the mass of the core exceeds the Chandrasekhar mass, electron pressure is no longer sufficient to balance gravitational contraction and the star evolves towards the formation of a neutron star or a black hole.

The formation of the core in massive stars is characterized by the appearance of neutrinos, produced in the process



Neutrinos do not have appreciable interactions with the surrounding matter and leave the core region carrying away energy. Thus, neutrino emission contributes to the collapse of the core. Other processes leading to a decrease of the pressure are electron capture



whose main effect is the disappearance of electrons carrying large kinetic energies, and

iron photodisintegration



which is an endothermic reaction.

Due to the combined effect of the above mechanisms, when the mass exceeds the Chandrasekhar limit, the core collapses within fractions of a second to reach densities  $\sim 10^{14} \text{ g/cm}^3$ , comparable with the central density of atomic nuclei.

At this stage the core behaves as a giant nucleus, made mostly of neutrons, and reacts elastically to further compression producing a strong shock wave which throws away a significant fraction of matter in the outer layers of the star. Nucleosynthesis of elements heavier than Iron is believed to take place during this explosive phase.

The above sequence of events leads to the appearance of a *supernova*, a star whose luminosity first grows fast, until it reaches a value exceeding sun luminosity by a factor  $\sim 10^9$ , and then decreases by a factor  $\sim 10^2$  within few months. The final result of the explosion is the formation of a *nebula*, whose center is occupied by the remnant of the core, i.e. a neutron star.

The existence of compact astrophysical objects made of neutrons was predicted by Bohr, Landau and Rosenfeld right after the discovery of the neutron, back in 1932. In 1934, Baade and Zwicky first suggested that a neutron star may be formed in the aftermath of a supernova explosion. Finally, in 1968 the newly observed pulsars, radio sources blinking on and off at a constant frequency, were identified with rotating neutron stars.

The results of a pioneering study, carried out in 1939 by Oppenheimer and Volkoff within the framework of general relativity, show that the mass of a star consisting of noninteracting neutrons cannot exceed  $\sim 0.8 M_\odot$ . The fact that this maximum mass, the analogue of the Chandrasekhar mass of white dwarfs, turns out to be much smaller than the observed neutron star masses (typically  $\sim 1.4 M_\odot$ ) clearly shows that neutron star equilibrium requires a pressure other than the degeneracy pressure, whose origin has to

be traced back to the nature of hadronic interactions.

Unfortunately, the need of including dynamical effects in the EOS is confronted with the complexity of the fundamental theory of strong interactions. As a consequence, all available description of the EOS of neutron star matter are obtained within models, based on the theoretical knowledge of the underlying dynamics and constrained, as much as possible, by empirical data.

The internal structure of a neutron star, schematically illustrated in Fig. 2.1, is believed to feature a sequence of layers of different composition.

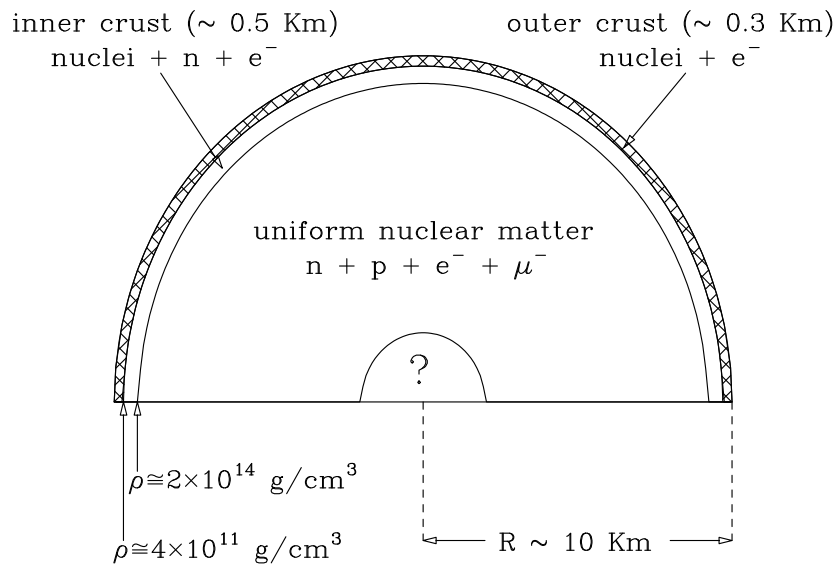


Figure 2.1: Schematic illustration of a neutron star cross section. Note that the equilibrium density of uniform nuclear matter corresponds to  $\sim 2.7 \times 10^{14} \text{g/cm}^3$ .

The properties of matter in the outer crust, corresponding to densities ranging from  $\sim 10^7 \text{g/cm}^3$  to the neutron drip density  $\rho_d = 4 \times 10^{11} \text{g/cm}^3$ , can be obtained directly from nuclear data. On the other hand, models of the EOS at  $4 \times 10^{11} < \rho < 2 \times 10^{14} \text{g/cm}^3$  are somewhat based on extrapolations of the available empirical information, as the extremely neutron rich nuclei appearing in this density regime are not observed on earth.

The density of the neutron star core ranges between  $\sim \rho_0 (= 2.67 \times 10^{14} \text{g/cm}^3)$  at the

boundary with the inner crust, and a central value that can be as large as  $1 \div 4 \times 10^{15} \text{ g/cm}^3$ . All models of EOS based on hadronic degrees of freedom predict that in the density range  $\rho_0 \lesssim \rho \lesssim 2\rho_0$  neutron star matter consists mainly of neutrons, with the admixture of a small number of protons, electrons and muons. At any given density the fraction of protons and leptons is determined by the requirements of equilibrium with respect to  $\beta$ -decay and charge neutrality.

This picture may change significantly at larger density with the appearance of heavy strange baryons produced in weak interaction processes. For example, although the mass of the  $\Sigma^-$  exceeds the neutron mass by more than 250 MeV, the reaction  $n + e^- \rightarrow \Sigma^- + \nu_e$  is energetically allowed as soon as the sum of the neutron and electron chemical potentials becomes equal to the  $\Sigma^-$  chemical potential.

Finally, as nucleons are known to be composite objects of size  $\sim 0.5 - 1.0 \text{ fm}$ , corresponding to a density  $\sim 10^{15} \text{ g/cm}^3$ , it is expected that if the density in the neutron star core reaches this value matter undergoes a transition to a new phase, in which quarks are no longer clustered into nucleons or hadrons.

The theoretical description of matter in the outer and inner neutron star crust will be outlined in the following Sections, whereas the region corresponding to supranuclear density will be discussed in Chapter 3.

## 2.2 Outer crust

A solid is expected to form when the ratio of Coulomb energy to thermal energy becomes large, i.e. when

$$\Gamma = \frac{Z^2 e^2}{T r_L} \gg 1, \quad (2.4)$$

with  $r_L$  defined through

$$n_I \frac{4\pi r_L^3}{3} = 1, \quad (2.5)$$

$n_I$  being the number density of ions. If the condition (2.4) is fulfilled Coulomb forces are weakly screened and become dominant, while the fluctuation of the ions is small compared to average ion spacing  $r_L$ . From (2.4) it follows that a solid is expected to form at temperature

$$T < T_m = \frac{Z^2 e^2}{r_L} \propto Z^2 e^2 n_I^{1/3} . \quad (2.6)$$

For example, in the case of  $^{56}\text{Fe}$  at densities  $\sim 10^7$  g/cm<sup>3</sup> solidification occurs at temperatures below  $10^8$  °K and Coulomb energy is minimized by a Body Centered Cubic (BCC) lattice. As the density further increases,  $r_L$  decreases, so that the condition for solidification continues to be fulfilled. However, as matter density advances into the density domain,  $10^7$  -  $10^{11}$  g/cm<sup>3</sup>, the large kinetic energy of the relativistic electrons shifts the energy balance, favouring inverse  $\beta$ -decay (i.e. electron capture) that leads to the appearance of new nuclear species through sequences like



This process is called neutronization, because the resulting nuclide is always richer in neutron content than the initial one.

Before going on with the analysis of the neutronization process in the neutron star crust, we will discuss a simple but instructive example, that will allow us to introduce some concepts and procedures to be used in the following Sections.

### 2.2.1 Inverse $\beta$ -decay

Consider a gas of noninteracting protons and electrons at  $T = 0$ . The neutronization process is due to the occurrence of weak interactions turning protons into neutrons through



Assuming neutrinos to be massless and non interacting, the above process is energetically favorable as soon as the electron energy becomes equal to the neutron-proton mass

difference

$$\Delta m = m_n - m_p = 939.565 - 938.272 = 1.293 \text{ MeV} . \quad (2.9)$$

As a consequence, the value of  $n_e$  at which inverse  $\beta$ -decay sets in can be estimated from

$$\sqrt{p_{F_e}^2 + m_e^2} = \Delta m , \quad (2.10)$$

where (see Section 1.2)

$$p_{F_e} = (3\pi^2 n_e)^{1/3} , \quad (2.11)$$

leading to

$$n_e = \frac{1}{3\pi^2} (\Delta m^2 - m_e^2)^{3/2} \approx 7 \times 10^{30} \text{ cm}^{-3} . \quad (2.12)$$

The corresponding mass density for a system having  $Y_e \sim 0.5$ , is  $\rho \approx 2.4 \times 10^7 \text{ g/cm}^3$ .

Now we want to address the problem of determining the ground state of the system consisting of protons, electrons and neutrons, once equilibrium with respect to the inverse  $\beta$ -decay of Eq. (2.8) has been reached. All interactions, except the weak interaction, will be neglected. Note that process (2.8) conserves the baryon number  $N_B$  (i.e. the baryon number density  $n_B$ ) and electric charge.

For any given value of  $n_B$ , the ground state is found by minimization of the total energy density of the systems,  $\epsilon(n_p, n_n, n_e)$ ,  $n_p$  and  $n_n$  being the proton and neutron density, respectively, with the constraints  $n_B = n_p + n_n$  (conservation of baryon number) and  $n_p = n_e$  (charge neutrality).

Let us define the function

$$F(n_p, n_n, n_e) = \epsilon(n_p, n_n, n_e) + \lambda_B (n_B - n_p - n_n) + \lambda_Q (n_p - n_e) , \quad (2.13)$$

where  $\epsilon$  is the energy density, while  $\lambda_B$  and  $\lambda_Q$  are Lagrange multipliers.

The minimum of  $F$  corresponds to the values of  $n_p$ ,  $n_n$  and  $n_e$  satisfying the conditions

$$\frac{\partial F}{\partial n_p} = \frac{\partial F}{\partial n_n} = 0 \quad , \quad \frac{\partial F}{\partial n_e} = 0 \quad (2.14)$$

as well as the additional constraints

$$\frac{\partial F}{\partial \lambda_B} = \frac{\partial F}{\partial \lambda_Q} = 0 . \quad (2.15)$$

From the definition of chemical potential of the particles of species  $i$  ( $i = p, n, e$ )

$$\mu_i = \left( \frac{\partial E}{\partial N_i} \right)_V = \left( \frac{\partial \epsilon}{\partial n_i} \right)_V \quad (2.16)$$

it follows that Eqs. (2.14) imply

$$\mu_p - \lambda_B + \lambda_Q = 0 \quad , \quad \mu_n - \lambda_B = 0 \quad , \quad \mu_e - \lambda_Q = 0 \quad , \quad (2.17)$$

leading to the condition of chemical equilibrium

$$\mu_n - \mu_p = \mu_e \quad , \quad (2.18)$$

where, in the case of noninteracting particles at  $T = 0$ ,

$$\begin{aligned} \mu_i &= \frac{\partial \epsilon}{\partial n_i} = \frac{2}{(2\pi)^3} \left( \frac{\partial p_{F_i}}{\partial n_i} \right) \frac{\partial}{\partial p_{F_i}} 4\pi \int_0^{p_{F_i}} p^2 dp \sqrt{p^2 + m_i^2} \\ &= \frac{8\pi}{(2\pi)^3} \left( \frac{\partial n_i}{\partial p_{F_i}} \right)^{-1} p_{F_i}^2 \sqrt{p_{F_i}^2 + m_i^2} = \sqrt{p_{F_i}^2 + m_i^2} . \end{aligned} \quad (2.19)$$

Defining now the proton and neutron fraction of the system as

$$x_p = \frac{n_p}{n_B} = \frac{n_p}{n_p + n_n} \quad , \quad x_n = \frac{n_n}{n_B} = 1 - x_p \quad (2.20)$$

we can rewrite

$$p_{F_p} = p_{F_e} = (3\pi^2 x_p n_B)^{1/3} \quad , \quad p_{F_n} = [3\pi^2 (1 - x_p) n_B]^{1/3} . \quad (2.21)$$

For fixed baryon density, use of the above definitions in Eq. (2.19) and substitution of the resulting chemical potentials into Eq. (2.18) leads to an equation in the single variable  $x_p$ . Hence, for any given  $n_B$  the requirements of chemical equilibrium and charge neutrality uniquely determine the fraction of protons in the system.

Once the value of  $x_p$  is known, the neutron, proton and electron number densities can be evaluated and the pressure

$$P = P_n + P_p + P_e \quad (2.22)$$

can be obtained using Eq. (1.27).

Figure 2.2.1 shows the proton and neutron number densities,  $n_p$  and  $n_n$  (recall that  $n_e = n_p$ ) as a function of matter density  $\rho$ . It can be seen that in the range  $10^5 \leq \rho \leq 10^7$  g/cm<sup>3</sup> there are protons only and  $\log n_p$  grows linearly with  $\log \rho$ . At  $\rho \sim 10^7$  g/cm<sup>3</sup> neutronization sets in and the neutron number density begins to steeply increase. At  $\rho > 10^7$   $n_p$  stays nearly constant, while neutrons dominate.

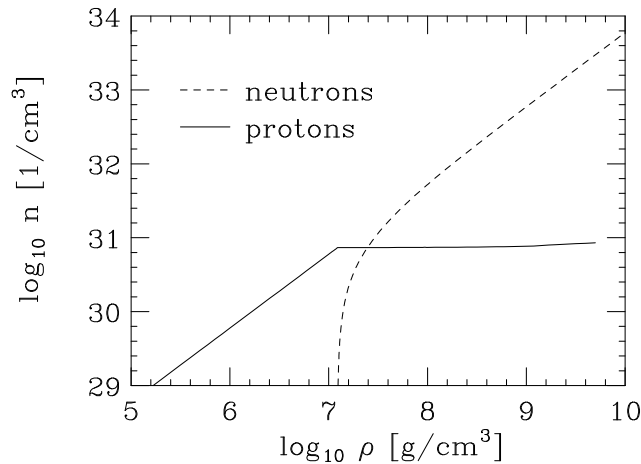


Figure 2.2: Number density of noninteracting protons and neutrons in  $\beta$ -equilibrium as a function of matter density.

The equation of state of the  $\beta$ -stable mixture is shown in the upper panel of Fig. 2.2.1. Its main feature is that pressure remains nearly constant as matter density increases by almost two orders of magnitude, in the range  $10^7 \leq \rho \leq 10^9$  g/cm<sup>3</sup>. The electron and neutron contributions to the pressure are shown in the lower panel of Fig. 2.2.1. Note that, since charge neutrality requires  $n_p = n_e$ , the proton pressure is smaller than the electron pressure by a factor  $(m_p/m_e) \sim 2000$ .



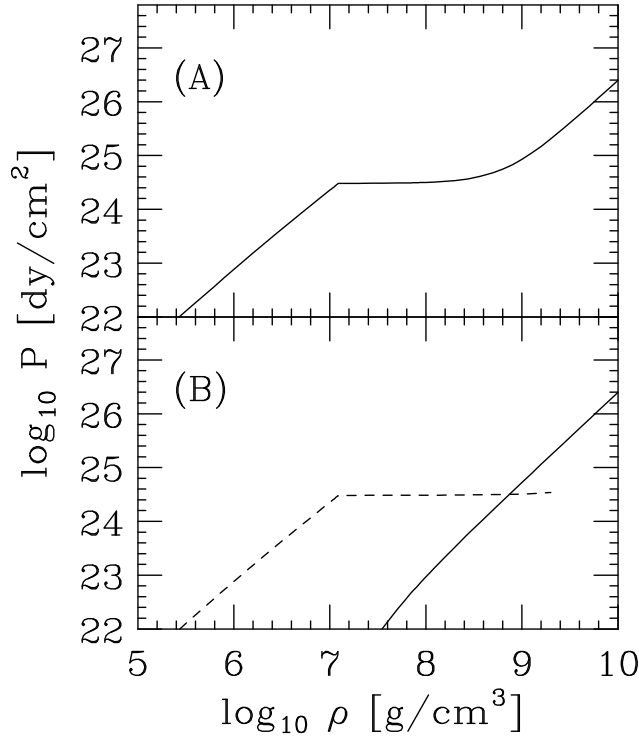


Figure 2.3: (A) Equation of state of a mixture of noninteracting neutrons, electrons and protons in  $\beta$ -equilibrium. (B) Density dependence of the neutron (solid line) and electron (dashed line) contributions to the pressure of  $\beta$ -stable matter.

### 2.2.2 Neutronization

The description of  $\beta$ -stable matter in terms of a mixture of degenerate Fermi gases of neutrons, protons and electrons is strongly oversimplified. In reality, electron capture changes a nucleus with given charge  $Z$  and mass number  $A$  into a different nucleus with the same  $A$  and charge  $(Z-1)$ . Moreover, the new nucleus may be metastable, so that two-step processes of the type



can take place. In this case, chemical equilibrium is driven by the mass difference between neighboring nuclei rather than the neutron-proton chemical potential difference.

The measured nuclear charge distributions and masses,  $\rho_{ch}(r)$  and  $M(Z, A)$ , exhibit

two very important features

- The charge density is nearly constant within the nuclear volume, its value being roughly the same for all stable nuclei, and drops from  $\sim 90\%$  to  $\sim 10\%$  of the maximum over a distance  $R_T \sim 2.5$  fm ( $1 \text{ fm} = 10 \times 10^{-13} \text{ cm}$ ), independent of  $A$ , called surface thickness (see Fig. 2.4). It can be parametrized in the form

$$\rho_{ch}(r) = \rho_0 \frac{1}{1 + e^{(r-R)/D}} , \quad (2.24)$$

where  $R = r_0 A^{1/3}$ , with  $r_0 = 1.07$  fm, and  $D = 0.54$  fm. Note that the nuclear charge radius is proportional to  $A^{1/3}$ , implying that the nuclear volume increases linearly with the mass number  $A$ .

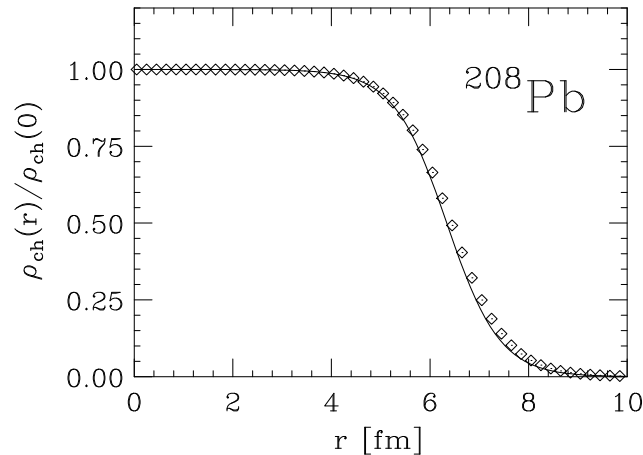


Figure 2.4: Nuclear charge distribution of  $^{208}\text{Pb}$ , normalized to  $Z/\rho(0)$  ( $Z = 82$ ). The solid line has been obtained using the parametrization of Eq. (2.24), while the diamonds represent the results of a model independent analysis of electron scattering data.

- The (positive) binding energy per nucleon, defined as

$$\frac{B(Z, A)}{A} = \frac{1}{A} [Zm_p + (A - Z)m_n + Zm_e - M(Z, A)] , \quad (2.25)$$

where  $M(Z, A)$  is the measured nuclear mass, is almost constant for  $A \geq 12$ , its value being  $\sim 8.5$  MeV (see Fig. 2.5).

The  $A$  and  $Z$  dependence of  $B(Z, A)$  can be parametrized according to the *semiempirical-mass formula*

$$\frac{B(Z, A)}{A} = \frac{1}{A} \left[ a_V A - a_s A^{2/3} - a_c \frac{Z^2}{A^{1/3}} - a_A \frac{(A - 2Z)^2}{4A} + \lambda a_p \frac{1}{A^{1/2}} \right]. \quad (2.26)$$

The first term in square brackets, proportional to  $A$ , is called the *volume term* and

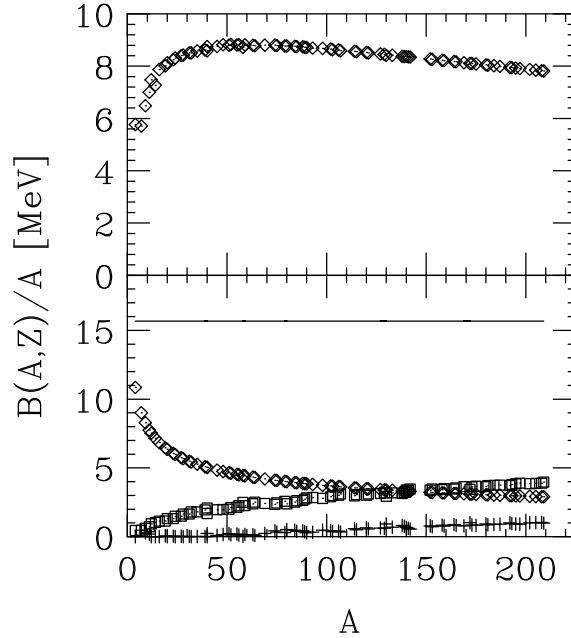


Figure 2.5: Upper panel:  $A$ -dependence of the binding energy per nucleon of stable nuclei, evaluated according to Eq. (2.26) with  $a_V = 15.67$  MeV,  $a_s = 17.23$  MeV,  $a_c = .714$  MeV,  $a_A = 93.15$  MeV and  $a_p = 11.2$  MeV. Lower panel: the solid line shows the magnitude of the volume contribution to the binding energy per nucleon, whereas the  $A$ -dependence of the surface, coulomb and symmetry contributions are represented by diamonds, squares and crosses, respectively.

describes the bulk energy of nuclear matter. The second term, proportional to the nuclear radius squared, is associated with the surface energy, while the third one accounts for the Coulomb repulsion between  $Z$  protons uniformly distributed within a sphere of radius  $R$ . The fourth term, that goes under the name of *symmetry energy* is required to describe

the experimental observation that stable nuclei tend to have the same number of neutrons and protons. Moreover, even-even nuclei (i.e. nuclei having even  $Z$  and even  $A - Z$ ) tend to be more stable than even-odd or odd-odd nuclei. This property is accounted for by the last term in the above equation, where  $\lambda = -1, 0$  and  $+1$  for even-even, even-odd and odd-odd nuclei, respectively. Fig. 2.5 shows the different contributions to  $B(Z, A)/A$ , evaluated using Eq. (2.26).

The semi-empirical nuclear mass formula of Eq. (2.26) can be used to obtain a qualitative description of the neutronization process. The total energy density of the system consisting of nuclei of mass number  $A$  and charge  $Z$  arranged in a lattice and surrounded by a degenerate electron gas is

$$\epsilon_T(n_B, A, Z) = \epsilon_e + \left(\frac{n_B}{A}\right) [M(Z, A) + \epsilon_L] , \quad (2.27)$$

where  $\epsilon_e$  is the energy density of the electron gas, Eq. (1.24),  $n_B$  and  $(n_B/A)$  denote the number densities of nucleons and nuclei, respectively, and  $\epsilon_L$  is the electrostatic lattice energy per site. As a first approximation, the contribution of  $\epsilon_L$  will be neglected.

At any given nucleon density  $n_B$  the equilibrium configuration corresponds to the values of  $A$  and  $Z$  that minimize  $\epsilon_T(n_B, A, Z)$ , i.e. to  $A$  and  $Z$  such that

$$\left(\frac{\partial \epsilon_T}{\partial Z}\right)_{n_B} = 0 , \quad \left(\frac{\partial \epsilon_T}{\partial A}\right)_{n_B} = 0 . \quad (2.28)$$

Combining the above relationships and using Eq. (2.26) one finds

$$Z \simeq 3.54 A^{1/2} . \quad (2.29)$$

Once  $Z$  is known as a function of  $A$ , any of the two relationships (2.28) can be used to obtain  $A$  as a function of  $n_B$ . The mass number  $A$  turns out to be an increasing function of  $n_B$ , implying that  $Z$  also increases with  $n_B$ , but at a slower rate. Hence, nuclei become more massive and more and more neutron rich as the nucleon density increases.

The above discussion is obviously still oversimplified. In reality,  $A$  and  $Z$  are *not* continuous variables and the total energy has to be minimized using the measured nuclear masses, rather than the parametrization of Eq. (2.26), and including the lattice energy, that can be written as

$$\epsilon_L = -K \frac{(Ze)^2}{r_s} \quad (2.30)$$

where  $r_s$  is related to the number density of nuclei through  $(4\pi/3)r_s^3 = (n_B/A)^{-1}$  and  $K = 0.89593$  for a BCC lattice, yielding the lowest energy. At fixed nucleon number density  $n_B$  the total energy density can be written in the form

$$\epsilon_T(n_B, A, Z) = \epsilon_e + \left(\frac{n_B}{A}\right) \left[ M(Z, A) - 1.4442(Ze)^2 \left(\frac{n_B}{A}\right)^{1/3} \right], \quad (2.31)$$

where, for matter density exceeding  $\sim 10^6$  g/cm<sup>3</sup>, the extreme relativistic limit of the energy density of an electron gas at number density  $n_e = Zn_B/A$  (see Section 1.2)

$$\epsilon_e = \frac{3}{4} \left( Z \frac{n_B}{A} \right)^{4/3}, \quad (2.32)$$

has to be used.

Collecting together the results of Eqs. (2.30)-(2.32) and expressing  $n_B$  in units of  $n_{B_0} = 10^{-9}$  fm<sup>-3</sup> (the number density corresponding to a matter density  $\sim 10^6$  g/cm<sup>3</sup>), the total *energy per nucleon*,  $\epsilon_T/n_B$ , can be rewritten in units of MeV as

$$\frac{\epsilon_T}{n_B} = \frac{M(Z, A)}{A} + \frac{1}{A^{4/3}} \left[ 0.4578 Z^{4/3} - \frac{Z^2}{480.74} \right] \left( \frac{n_B}{n_{B_0}} \right)^{1/3}. \quad (2.33)$$

The average energy per nucleon in a nucleus is about 930 MeV. It can be conveniently written in units of MeV in the form  $M(Z, A)/A = 930 + \Delta$ . As long as we are dealing with nuclides that are not very different from the stable nuclides, the values of  $\Delta$  are available in form of tables based on actual measurements or extrapolations of the experimental data.

In practice,  $\epsilon_T/n_B$  of Eq. (2.33) is computed for a given nucleus (i.e. for given  $A$  and  $Z$ ) as a function of  $n_B$ , and plotted versus  $1/n_B$  (see Fig. 2.6). The curves corresponding

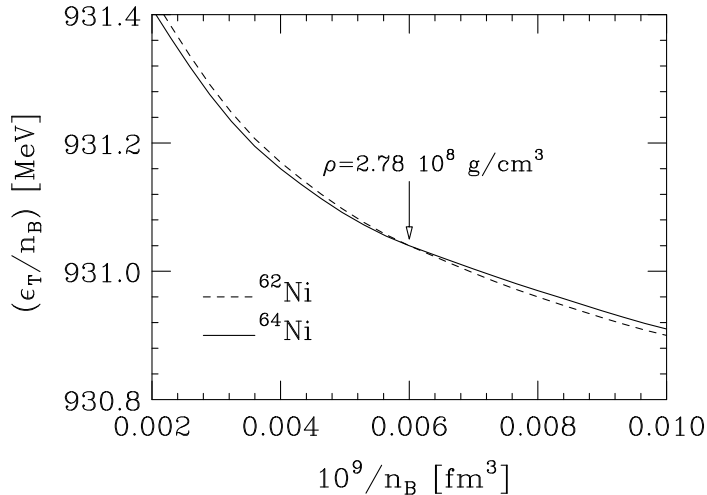


Figure 2.6: Total energy per nucleon of a BCC lattice of  $^{62}\text{Ni}$  (dashed line) and  $^{64}\text{Ni}$  (solid line) nuclei surrounded by an electron gas, evaluated using eq.(2.33) and plotted versus the inverse nucleon number density.

to different nuclei are then compared and the nucleus corresponding to the minimum energy at given  $n_B$  can be easily identified. For example, the curves of Fig. 2.6 show the behavior of the energy per particle corresponding to  $^{62}\text{Ni}$  and  $^{64}\text{Ni}$ , having  $A-Z = 34$  and  $36$ , respectively. It is apparent that a first order phase transition is taking place around the point where the two curves cross one another. The exact densities at which the phase transition occurs and terminates can be obtained using Maxwell's double tangent construction. This method essentially amounts to drawing a straight line tangent to the convex curves corresponding to the two nuclides. In a first order phase transition the pressure remains constant as the density increases. Hence, as all points belonging to the tangent of Maxwell's construction correspond to the same pressure, the onset and termination of the phase transition are simply given by the points of tangency. As expected, at higher density the nucleus with the largest number of neutrons yields a lower energy.

It has to be pointed out that there are limitations to the approach described in this

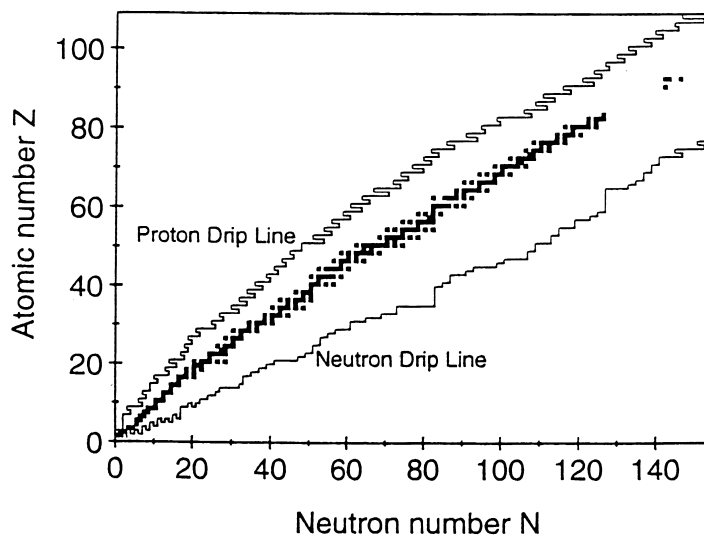


Figure 2.7: Chart of the nuclides. The black squares represent the stable nuclei as a function of  $Z$  and  $N=A-Z$ . The solid lines correspond to the estimated proton and neutron drip lines.

section. Some of the nuclides entering the minimization procedure have ratios  $Z/A$  so different from those corresponding to stable nuclei (whose typical value of  $Z/A$  is  $\sim 0.5$ , as shown in Fig. 2.7) that the accuracy of the extrapolated masses may be questionable. Obviously, this problem becomes more and more important as the density increases. The study of nuclei far from stability, carried out with radioactive nuclear beams, is regarded as one of the highest priorities in nuclear physics research, and new dedicated experimental facilities are currently being planned both in the U.S. and in Europe.

Table 2.1 reports the sequence of nuclides corresponding to the ground state of matter at subnuclear density, as a function of matter density.

## 2.3 Inner crust

Table 2.1 shows that as the density increases the nuclides corresponding to the ground state of matter become more and more neutron rich. At  $\rho \sim 4.3 \times 10^{11} \text{ g/cm}^3$  the ground state corresponds to a Coulomb lattice of  $^{118}\text{Kr}$  nuclei, having proton to neutron ratio

Nuclide	Z	N = A - Z	Z/A	$\Delta$ [MeV]	$\rho_{max}$ [g/cm <sup>3</sup> ]
<sup>56</sup> Fe	26	30	.4643	.1616	$8.1 \times 10^6$
<sup>62</sup> Ni	28	34	.4516	.1738	$2.7 \times 10^8$
<sup>64</sup> Ni	28	36	.4375	.2091	$1.2 \times 10^9$
<sup>84</sup> Se	34	50	.4048	.3494	$8.2 \times 10^9$
<sup>82</sup> Ge	32	50	.3902	.4515	$2.1 \times 10^{10}$
<sup>84</sup> Zn	30	54	.3750	.6232	$4.8 \times 10^{10}$
<sup>78</sup> Ni	28	50	.3590	.8011	$1.6 \times 10^{11}$
<sup>76</sup> Fe	26	50	.3421	1.1135	$1.8 \times 10^{11}$
<sup>124</sup> Mo	42	82	.3387	1.2569	$1.9 \times 10^{11}$
<sup>122</sup> Zr	40	82	.3279	1.4581	$2.7 \times 10^{11}$
<sup>120</sup> Sr	38	82	.3166	1.6909	$3.7 \times 10^{11}$
<sup>118</sup> Kr	36	82	.3051	1.9579	$4.3 \times 10^{11}$

Table 2.1: Sequence of nuclei corresponding to the ground state of matter and maximum density at which they occur. Nuclear masses are given by  $M(Z,A)/A = (930 + \Delta)$  MeV.

$\sim 0.31$  and a slightly negative neutron chemical potential (i.e. neutron Fermi energy), surrounded by a degenerate electron gas with chemical potential  $\mu_e \sim 26$  MeV. At larger densities a new regime sets in, since the neutrons created by electron capture occupy positive energy states and begin to *drip* out of the nuclei, filling the space between them.

At these densities the ground state corresponds to a mixture of two phases: matter consisting of neutron rich nuclei (phase I), with density  $\rho_{nuc}$ , and a neutron gas of density  $\rho_{NG}$  (phase II).

The equilibrium conditions are

$$(\mu_n)_I = (\mu_n)_{II} = \mu_n \quad (2.34)$$

and

$$\mu_p = \mu_n - \mu_e, \quad (2.35)$$



where  $(\mu_n)_I$  and  $(\mu_n)_{II}$  denote the neutron chemical potential in the neutron gas and in the matter of nuclei, respectively.

The details of the ground state of matter in the neutron drip regime are specified by the densities  $\rho$ ,  $\rho_{\text{nuc}}$  and  $\rho_{\text{NG}}$ , the proton to neutron ratio of the matter in phase I and its surface, whose shape is dictated by the interplay between surface and Coulomb energies.

Recent studies suggest that at densities  $4.3 \times 10^{10} \lesssim \rho \lesssim .75 \times 10^{14} \text{ g/cm}^3$  the matter in phase I is arranged in spheres immersed in electron and neutron gas, whereas at  $.75 \times 10^{14} \lesssim \rho \lesssim 1.2 \times 10^{14} \text{ g/cm}^3$  the energetically favoured configurations exhibit more complicated structures, featuring rods of matter in phase I or alternating layers of matter in phase I and phase II. At  $\rho \gtrsim 1.2 \times 10^{14} \text{ g/cm}^3$  there is no separation between the phases, and the ground state of matter corresponds to a homogeneous fluid of neutrons, protons and electrons.



# Chapter 3

## Nuclear matter Matter in the the neutron star interior

### 3.1 Nuclear matter at supranuclear densities

Understanding the properties of matter at densities comparable to the central density of atomic nuclei ( $\rho_0 \sim 2.7 \times 10^{14} \text{ g/cm}^3$ ) is made difficult by *both* the complexity of the interactions *and* the approximations implied in the theoretical description of quantum mechanical many particle systems. The situation becomes even more problematic as we enter the region of *supranuclear* density, corresponding to  $\rho > \rho_0$ , as the available empirical information is scarce, and one has to unavoidably resort to a mixture of extrapolation and speculation.

The approach based on nonrelativistic quantum mechanics and phenomenological nuclear hamiltonians, while allowing for a rather satisfactory description of nuclear bound states and nucleon-nucleon scattering data, fails to fulfill the constraint of causality, as it leads to predict a speed of sound in matter that exceeds the speed of light at large density. On the other hand, the approach based on relativistic quantum field theory, while fulfilling the requirement of causality by construction, assumes a somewhat oversimplified dynamics, not constrained by nucleon-nucleon data. In addition, it is plagued by the uncertainty associated with the use of the mean field approximation, which is long known

to fail in strongly correlated systems.

In this Chapter, after reviewing the phenomenological constraints on the EOS of cold nuclear matter, we will outline the current understanding of the nucleon-nucleon interaction and the nonrelativistic and relativistic approaches employed to study the structure of neutron star matter at nuclear and supernuclear density. As anticipated in Section 2.1, in this region a neutron star is believed to consist of a uniform fluid of neutrons, protons and electrons in  $\beta$ -equilibrium.

## 3.2 Constraints on the nuclear matter EOS

The body of data on nuclear masses can be used to constrain the density dependence predicted by theoretical models of uniform nuclear matter at zero temperature.

As we have seen in Section 2.2.2, the  $A$ -dependence of the nuclear binding energy is well described by the semiempirical formula (2.26). In the large  $A$  limit and neglecting the effect of Coulomb repulsion between protons, the only term surviving in the case  $Z = A/2$  is the term linear in  $A$ . Hence, the coefficient  $a_V$  can be identified with the binding energy per particle of *symmetric nuclear matter*, an ideal uniform system consisting of equal number of protons and neutrons coupled by strong interactions only. The equilibrium density of such a system,  $n_0$ , can be inferred exploiting saturation of nuclear densities, i.e. the fact that the central density of atomic nuclei, measured by elastic electron-nucleus scattering, does not depend upon  $A$  for large  $A$  (see Fig. 3.1).

The empirical equilibrium properties of symmetric nuclear matter are

$$\left(\frac{E}{A}\right)_{n=n_0} = -16 \text{ MeV} \quad , \quad n_0 \sim .16 \text{ fm}^{-3} . \quad (3.1)$$

In the vicinity of the equilibrium density  $e = E/A$  can be expanded according to

$$e(n) \approx e_0 + \frac{1}{2} \frac{K}{9} \frac{(n - n_0)^2}{n_0^2} , \quad (3.2)$$

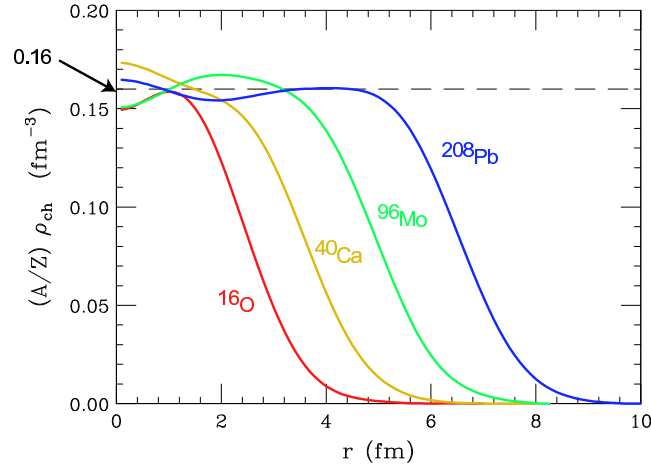


Figure 3.1: Saturation of central nuclear densities measured by elastic electron-nucleus scattering.

where

$$K = 9 n_0^2 \left( \frac{\partial^2 e}{\partial n^2} \right)_{n=n_0} = 9 \left( \frac{\partial P}{\partial n} \right)_{n=n_0} \quad (3.3)$$

is the (in)compressibility module, that can be extracted from the measured excitation energies of nuclear vibrational states. Due to the difficulties implied in the analysis of these experiments, however, empirical estimates of  $K$  have a rather large uncertainty, and range from  $\sim 200$  MeV (corresponding to more compressible nuclear matter, i.e. to a *soft* EOS) to  $\sim 300$  MeV (corresponding to a *stiff* EOS).

Unfortunately, the quadratic extrapolation of Eq. (3.2) cannot be expected to work far from equilibrium density. In fact, assuming a parabolic behavior of  $e(n)$  at large  $n$  ( $\gg n_0$ ) leads to predict a speed of sound in matter,  $c_s$ , larger than the speed of light, i.e. (compare to Eq. (1.42))

$$c_s^2 = \frac{1}{n} \left( \frac{\partial P}{\partial e} \right) > 1, \quad (3.4)$$

regardless of the value of  $K$ .

Equation (3.4) shows that causality requires

$$\left( \frac{\partial P}{\partial \epsilon} \right) < 1, \quad (3.5)$$

$\epsilon$  being the energy-density. For a noninteracting Fermi gas  $\epsilon \propto n^{4/3}$ , implying (the equal sign corresponds to massless fermions)

$$P \leq \frac{\epsilon}{3} \quad , \quad c_s \leq \frac{1}{3} . \quad (3.6)$$

In presence of interactions the above limits can be easily exceeded. For example, modeling the repulsion between nucleons in terms of a rigid core leads to predict infinite pressure at finite density.

The relation between microscopic dynamics and speed of sound in matter has been studied by Zel'dovich in the early 60s within the framework of relativistic quantum field theory.

Assuming that the energy density be related to number density through the power law

$$\epsilon = \frac{E}{V} = an^\nu \quad , \quad (3.7)$$

energy per particle and pressure can be written

$$e = \frac{E}{N} = a\nu^{n-1} \quad , \quad (3.8)$$

$$P = n^2 \left( \frac{\partial e}{\partial n} \right) = (n-1)an^\nu = (n-1)\epsilon . \quad (3.9)$$

From the above relations we easily see that that  $\nu = 4/3$  corresponds to  $P = \epsilon/3$  and that the limiting case  $c_s = 1$ , i.e.  $(\partial P)/(\partial \epsilon) = 1$  is reached when  $\nu = 2$ . Powers higher than  $\nu = 2$  are forbidden by causality.

In the model proposed by Zel'dovich matter consists of baryons interacting through exchange of a massive vector meson described by the lagrangian density

$$\mathcal{L}_V = -\frac{1}{4}F_{\mu\nu}F^{\mu\nu} - \frac{1}{2}\mu^2 A_\mu A^\mu \quad (3.10)$$

where  $A^\mu \equiv (\phi, \mathbf{A})$  and  $\mu$  is the meson mass. The corresponding field equation is

$$(\partial^\nu \partial_\nu + \mu^2)A_\mu = gJ_\mu \quad , \quad (3.11)$$

$g$  being the coupling constant. In the simple case of a point source located at  $\mathbf{x} = 0$

$$J_\mu \equiv (J_0, \mathbf{J}) \equiv (\delta(\mathbf{x}), 0) \quad (3.12)$$

and the solution of (3.11) is

$$\phi(\mathbf{x}') = g \frac{e^{-\mu|\mathbf{x}'-\mathbf{x}|}}{|\mathbf{x}'-\mathbf{x}|}, \quad \mathbf{A} = 0. \quad (3.13)$$

Two charges at rest separated by a distance  $r$  repel each other with a force of magnitude

$$F = -g^2 \frac{d}{dr} \frac{e^{-\mu r}}{r} \quad (3.14)$$

and the corresponding interaction energy is

$$g\phi = g^2 \frac{e^{-\mu r}}{r}. \quad (3.15)$$

In the case of  $N$  particles of mass  $M$ , as the equation of motion (3.11) is linear, we can use the superposition principle and write the total energy as ( $r_{ij} = |\mathbf{r}_i - \mathbf{r}_j|$ )

$$E = NM + g^2 \sum_{j>i=1}^N \frac{e^{-\mu r_{ij}}}{r_{ij}}. \quad (3.16)$$

Let us now make the further assumption that the average particle density be such that

$$\left(\frac{1}{n}\right)^{1/3} < \frac{1}{\mu}. \quad (3.17)$$

The above equation implies that the meson field changes slowly over distances comparable to the average particle separation. If this is the case we can use the mean field approximation and rewrite Eq. (3.16) in the form

$$e = \frac{E}{N} = M + \frac{g^2}{2} \int d^3r \frac{e^{-\mu r}}{r} = m + 2\pi g^2 \frac{n}{\mu}. \quad (3.18)$$

The corresponding expression of the energy density and pressure read

$$\epsilon = ne = nM + 2\pi g^2 \frac{n^2}{\mu} \quad (3.19)$$

and

$$P = n^2 \left( \frac{\partial e}{\partial n} \right) = 2\pi g^2 \frac{n^2}{\mu} . \quad (3.20)$$

From the above equations it follows that, in the large  $n$  limit  $P \rightarrow \epsilon$ , implying in turn  $c_s \rightarrow 1$ .

In conclusion, Zel'dovich model shows that the causality limit, corresponding to  $\epsilon \propto n^2$ , is indeed attained in a simple semirealistic theory, in which nucleons are assumed to interact through exchange of a vector meson.

### 3.3 The nucleon-nucleon interaction

The main features of the nucleon-nucleon (NN) interaction, inferred from the analysis of nuclear systematics, may be summarized as follows.

- The *saturation* of nuclear density (see Fig. 3.1), i.e. the fact that density in the interior of atomic nuclei is nearly constant and independent of the mass number  $A$ , tells us that nucleons cannot be packed together too tightly. Hence, at short distance the NN force must be repulsive. Assuming that the interaction can be described by a nonrelativistic potential  $v$  depending on the interparticle distance,  $\mathbf{r}$ , we can then write:

$$v(\mathbf{r}) > 0 \quad , \quad |\mathbf{r}| < r_c , \quad (3.21)$$

$r_c$  being the radius of the repulsive core.

- The fact that the nuclear binding energy per nucleon is roughly the same for all nuclei with  $A \geq 20$ , its value being

$$\frac{B(Z, A)}{A} \sim 8.5 \text{ MeV} , \quad (3.22)$$

suggests that the NN interaction has a finite range  $r_0$ , i.e. that

$$v(\mathbf{r}) = 0 \quad , \quad |\mathbf{r}| > r_0 . \quad (3.23)$$



- The spectra of the so called *mirror nuclei*, i.e. pairs of nuclei having the same  $A$  and charges differing by one unit (implying that the number of protons in a nucleus is the same as the number of neutrons in its mirror companion), e.g.  ${}^{15}_7\text{N}$  ( $A = 15$ ,  $Z = 7$ ) and  ${}^{15}_8\text{O}$  ( $A = 15$ ,  $Z = 8$ ), exhibit striking similarities. The energies of the levels with the same parity and angular momentum are the same up to small electromagnetic corrections, showing that protons and neutrons have similar nuclear interactions, i.e. that nuclear forces are *charge symmetric*.

Charge symmetry is a manifestation of a more general property of the NN interaction, called *isotopic invariance*. Neglecting the small mass difference, proton and neutron can be viewed as two states of the same particle, the nucleon (N), described by the Dirac equation obtained from the lagrangian density

$$\mathcal{L} = \bar{\psi}_N (i\gamma^\mu \partial_\mu - m) \psi_N \quad (3.24)$$

where

$$\psi_N = \begin{pmatrix} p \\ n \end{pmatrix}, \quad (3.25)$$

$p$  and  $n$  being the four-spinors associated with the proton and the neutron, respectively. The lagrangian density (3.24) is invariant under the SU(2) global phase transformation

$$U = e^{i\alpha_j \tau_j}, \quad (3.26)$$

where  $\alpha$  is a constant (i.e. independent of  $x$ ) vector and the  $\tau_j$  ( $j = 1, 2, 3$ ) are Pauli matrices. The above equations show that the nucleon can be described as a doublet in isospin space. Proton and neutron correspond to isospin projections  $+1/2$  and  $-1/2$ , respectively. Proton-proton and neutron-neutron pairs always have total isospin  $T=1$  whereas a proton-neutron pair may have either  $T = 0$  or  $T = 1$ . The two-nucleon isospin

states  $|T, T_3\rangle$  can be summarized as follows

$$\begin{aligned} |1, 1\rangle &= |pp\rangle \\ |1, 0\rangle &= \frac{1}{\sqrt{2}} (|pn\rangle + |np\rangle) \\ |1, -1\rangle &= |nn\rangle \\ |0, 0\rangle &= \frac{1}{\sqrt{2}} (|pn\rangle - |np\rangle) . \end{aligned}$$

Isospin invariance implies that the interaction between two nucleons separated by a distance  $r = |\mathbf{r}_1 - \mathbf{r}_2|$  and having total spin  $S$  depends on their total isospin  $T$  but not on  $T_3$ . For example, the potential  $v(\mathbf{r})$  acting between two protons with spins coupled to  $S = 0$  is the same as the potential acting between a proton and a neutron with spins and isospins coupled to  $S = 0$  and  $T = 1$ .

### 3.4 The two-nucleon system

The details of the NN interaction can be best studied in the two-nucleon system. There is *only one* NN bound state, the nucleus of deuterium, or deuteron ( ${}^2\text{H}$ ), consisting of a proton and a neutron coupled to total spin and isospin  $S = 1$  and  $T = 0$ , respectively. This is clear manifestation of the fact that nuclear forces are *spin dependent*.

Another important piece of information can be inferred from the observation that the deuteron exhibits a nonvanishing electric quadrupole moment, implying that its charge distribution is not spherically symmetric. Hence, the NN interaction is *noncentral*.

Besides the properties of the two-nucleon bound state, the large data base of phase shifts measured in NN scattering experiments ( $\sim 4000$  data points corresponding to energies up to 350 MeV in the lab frame) provides valuable additional information on the nature of NN forces.

The theoretical description of the NN interaction was first attempted by Yukawa in 1935. He made the hypothesis that nucleons interact through the exchange of a particle,

whose mass  $\mu$  can be related to the interaction range  $r_0$  according to

$$r_0 \sim \frac{1}{\mu} . \quad (3.27)$$

Using  $r_0 \sim 1$  fm, the above relation yields  $\mu \sim 200$  MeV (1 fm = 197.3 MeV).

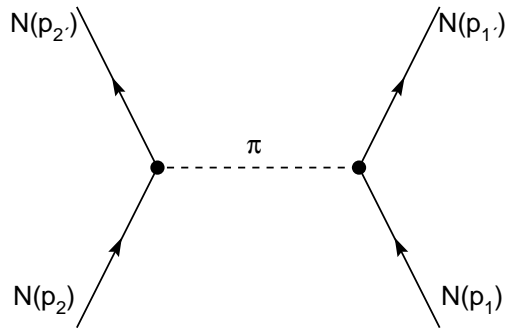


Figure 3.2: Feynman diagram describing the one-pion-exchange process between two nucleons. The corresponding amplitude is given by Eq. (3.28).

Yukawa's idea has been successfully implemented identifying the exchanged particle with the  $\pi$  meson (or *pion*), discovered in 1947, whose mass is  $m_\pi \sim 140$  MeV. Experiments show that the pion is a spin zero pseudoscalar particle <sup>1</sup> (i.e. it has spin-parity  $0^-$ ) that comes in three charge states, denoted  $\pi^+$ ,  $\pi^-$  and  $\pi^0$ . Hence, it can be regarded as an isospin  $T=1$  triplet, the charge states being associated with isospin projections  $T_3=+1$ , 0 and  $-1$ , respectively.

The simplest  $\pi$ -nucleon coupling compatible with the observation that nuclear interactions conserve parity has the pseudoscalar form  $ig\gamma^5\boldsymbol{\tau}$ , where  $g$  is a coupling constant and  $\boldsymbol{\tau}$  describes the isospin of the nucleon. With this choice for the interaction vertex, the amplitude of the process depicted in Fig. 3.2 can readily be written, using standard

---

<sup>1</sup>The pion spin has been deduced from the balance of the reaction  $\pi^+ + {}^2\text{H} \leftrightarrow p + p$ , while its intrinsic parity was determined observing the  $\pi^-$  capture from the K shell of the deuterium atom, leading to the appearance of two neutrons:  $\pi^- + d \rightarrow n + n$ .

Feynman's diagram techniques, as

$$\langle f|M|i\rangle = -ig^2 \frac{\bar{u}(p'_2, s'_2)\gamma_5 u(p_2, s_2)\bar{u}(p'_1, s'_1)\gamma_5 u(p_1, s_1)}{k^2 - m_\pi^2} \langle \boldsymbol{\tau}_1 \cdot \boldsymbol{\tau}_2 \rangle, \quad (3.28)$$

where  $k = p'_1 - p_1 = p_2 - p'_2$ ,  $k^2 = k_\mu k^\mu = k_0^2 - |\vec{k}|^2$ ,  $u(p, s)$  is the Dirac spinor associated with a nucleon of four momentum  $p \equiv (\vec{p}, E)$  ( $E = \sqrt{\mathbf{p}^2 + m^2}$ ) and spin projection  $s$  and

$$\langle \boldsymbol{\tau}_1 \cdot \boldsymbol{\tau}_2 \rangle = \eta_2^\dagger \boldsymbol{\tau} \eta_2 \eta_1^\dagger \boldsymbol{\tau} \eta_1, \quad (3.29)$$

$\eta_i$  being the two-component Pauli spinor describing the isospin state of particle  $i$ .

In the nonrelativistic limit, Yukawa's theory leads to define a NN interaction potential that can be written in coordinate space as

$$\begin{aligned} v_\pi &= \frac{g^2}{4m^2} (\boldsymbol{\tau}_1 \cdot \boldsymbol{\tau}_2) (\boldsymbol{\sigma}_1 \cdot \boldsymbol{\nabla}) (\boldsymbol{\sigma}_2 \cdot \boldsymbol{\nabla}) \frac{e^{-m_\pi r}}{r} \\ &= \frac{g^2}{(4\pi)^2} \frac{m_\pi^3}{4m^2} \frac{1}{3} (\boldsymbol{\tau}_1 \cdot \boldsymbol{\tau}_2) \left\{ \left[ (\boldsymbol{\sigma}_1 \cdot \boldsymbol{\sigma}_2) + S_{12} \left( 1 + \frac{3}{x} + \frac{3}{x^2} \right) \right] \frac{e^{-x}}{x} \right. \\ &\quad \left. - \frac{4\pi}{\mu^3} (\boldsymbol{\sigma}_1 \cdot \boldsymbol{\sigma}_2) \delta^{(3)}(\mathbf{r}) \right\}, \end{aligned} \quad (3.30)$$

where  $x = m_\pi |\mathbf{r}|$  and

$$S_{12} = \frac{3}{r^2} (\boldsymbol{\sigma}_1 \cdot \mathbf{r}) (\boldsymbol{\sigma}_2 \cdot \mathbf{r}) - (\boldsymbol{\sigma}_1 \cdot \boldsymbol{\sigma}_2), \quad (3.31)$$

is reminiscent of the operator describing the noncentral interaction between two magnetic dipoles.

For  $g^2/(4\pi) = 14$ , the above potential provides an accurate description of the long range part ( $|\mathbf{r}| > 1.5$  fm) of the NN interaction, as shown by the very good fit of the NN scattering phase shifts in states of high angular momentum. In these states, due to the strong centrifugal barrier, the probability of finding the two nucleons at small relative distances becomes in fact negligibly small.

At medium- and short-range other more complicated processes, involving the exchange of two or more pions (possibly interacting among themselves) or heavier particles (like the

$\rho$  and the  $\omega$  mesons, whose masses are  $m_\rho = 770$  MeV and  $m_\omega = 782$  MeV, respectively), have to be taken into account. Moreover, when their relative distance becomes very small ( $|\mathbf{r}| \lesssim 0.5$  fm) nucleons, being composite and finite in size, are expected to overlap. In this regime, NN interactions should in principle be described in terms of interactions between nucleon constituents, i.e. quarks and gluons, as dictated by *quantum chromodynamics* (QCD), which is believed to be the fundamental theory of strong interactions.

Phenomenological potentials describing the *full* NN interaction are generally written as

$$v = \tilde{v}_\pi + v_R \quad (3.32)$$

where  $\tilde{v}_\pi$  is the one pion exchange potential, defined by Eqs. (3.30) and (3.31), stripped of the  $\delta$ -function contribution, whereas  $v_R$  describes the interaction at medium and short range. The spin-isospin dependence and the noncentral nature of the NN interactions can be properly described rewriting Eq. (3.32) in the form

$$v_{ij} = \sum_{ST} [v_{TS}(r_{ij}) + \delta_{S1} v_{tT}(r_{ij}) S_{12}] P_S \Pi_T, \quad (3.33)$$

$S$  and  $T$  being the total spin and isospin of the interacting pair, respectively. In the above equation  $P_S$  ( $S = 0, 1$ ) are the spin projection operators

$$P_0 = \frac{1}{4} (1 - \boldsymbol{\sigma}_1 \cdot \boldsymbol{\sigma}_2) \quad , \quad P_1 = \frac{1}{4} (3 + \boldsymbol{\sigma}_1 \cdot \boldsymbol{\sigma}_2) \quad , \quad (3.34)$$

satisfying

$$P_0 + P_1 = 1 \quad , \quad P_S |S'\rangle = \delta_{SS'} |S'\rangle \quad , \quad P_S P_{S'} = P_S \delta_{SS'} \quad , \quad (3.35)$$

and  $\Pi_T$  are the isospin projection operators that can be written as in Eq. (3.34) replacing  $\boldsymbol{\sigma} \rightarrow \boldsymbol{\tau}$ . The functions  $v_{TS}(r_{ij})$  and  $v_{tT}(r_{ij})$  describe the radial dependence of the interaction in the different spin-isospin channels and reduce to the corresponding components of the one pion exchange potential at large  $r_{ij}$ . Their shapes are chosen in such a way as to

reproduce the available NN data (deuteron binding energy, charge radius and quadrupole moment and the NN scattering phase shifts).

Substitution of Eq. (3.34) and the corresponding expressions for the isospin projection operators allows one to rewrite Eq. (3.33) in the form

$$v_{ij} = \sum_{n=1}^6 v^{(n)}(r_{ij}) O_{ij}^{(n)} , \quad (3.36)$$

where

$$O_{ij}^{(n)} = 1, (\boldsymbol{\tau}_i \cdot \boldsymbol{\tau}_j), (\boldsymbol{\sigma}_i \cdot \boldsymbol{\sigma}_j), (\boldsymbol{\sigma}_i \cdot \boldsymbol{\sigma}_j)(\boldsymbol{\tau}_i \cdot \boldsymbol{\tau}_j), S_{ij}, S_{ij}(\boldsymbol{\tau}_i \cdot \boldsymbol{\tau}_j) \quad (3.37)$$

and the  $v^{(n)}(r_{ij})$  are linear combination of the  $v_{TS}(r_{ij})$  and  $v_{tT}(r_{ij})$ . Note that the operators defined in Eq. (3.37) form an algebra, as they satisfy the relation

$$O_{ij}^{(n)} O_{ij}^{(m)} = \sum_{\ell} K_{nm\ell} O_{ij}^{(\ell)} , \quad (3.38)$$

where the coefficients  $K_{nm\ell}$  can be easily obtained from the properties of Pauli matrices. Equations (3.38) can be exploited to greatly simplify the calculation of nuclear observables based on the representation (3.36)-(3.37) of the NN potential.

The typical shape of the NN potential in the state of relative angular momentum  $\ell = 0$  and total spin and isospin  $S = 0$  and  $T = 1$  is shown in Fig. 3.3. The short range repulsive core, to be ascribed to heavy meson exchange or to more complicated mechanisms involving nucleon constituents, is followed by an intermediate range attractive region, largely due to two-pion exchange processes. Finally, at large interparticle distance the one-pion-exchange mechanism dominates. Note the similarity with the van der Waals potential of Fig. 1.1.

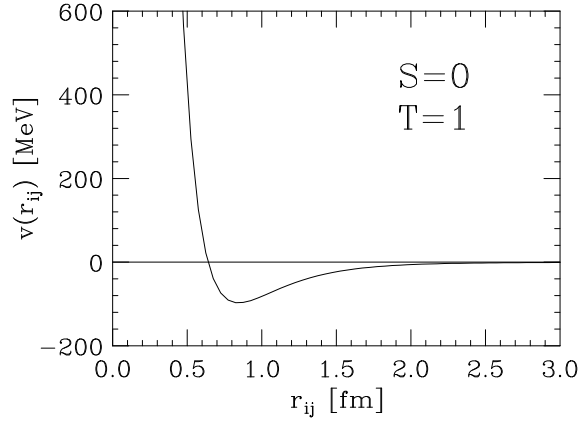


Figure 3.3: Radial dependence of the NN potential describing the interaction between two nucleons in the state of relative angular momentum  $\ell = 0$ , and total spin and isospin  $S = 0$  and  $T = 1$ .

### 3.5 Nonrelativistic many-body theory

Within nonrelativistic many-body theory (NMBT), nuclear systems are described as a collection of pointlike nucleons interacting through the hamiltonian

$$H = \sum_{i=1}^A \frac{\mathbf{p}_i^2}{2m} + \sum_{j>i=1}^A v_{ij} + \dots, \quad (3.39)$$

where  $\mathbf{p}_i$  denotes the momentum carried by the  $i$ -th nucleon,  $v_{ij}$  is the two-body potential describing NN interactions and the ellipsis refers to the possible existence of interactions involving more than two nucleons.

Unfortunately, solving the Schrödinger equation

$$H|\Psi_0\rangle = E_0|\Psi_0\rangle \quad (3.40)$$

for the ground state of a nucleus, using the hamiltonian (3.39) and the NN potential of Eqs.(3.36) and (3.37), is only possible for not too large  $A$ . The numerical solution is trivial for  $A=2$  only. For  $A=3$  Eq. (3.40) can still be solved using deterministic approaches, while for  $A>3$  sthochastic methods, such as the Green Function Monte Carlo method, have to be employed. The results of these calculations will be briefly reviewed in the next Section.

### 3.5.1 The few-nucleon systems

The NN potential determined from the properties of the two-nucleon system can be used to solve Eq. (3.40) for  $A > 2$ . In the case  $A = 3$  the problem can be still solved exactly, but the resulting ground state energy,  $E_0$ , turns out to be slightly different from the experimental value. For example, for  ${}^3He$  one typically finds  $E_0 = 7.6$  MeV, to be compared to  $E_{exp} = 8.48$  MeV. In order to exactly reproduce  $E_{exp}$  one has to add to the nuclear hamiltonian a term containing three-nucleon interactions described by a potential  $V_{ijk}$ . The most important process leading to three nucleon interactions is the two-pion exchange associated with the excitation of a nucleon resonance in the intermediate state, depicted in Fig. 3.4.

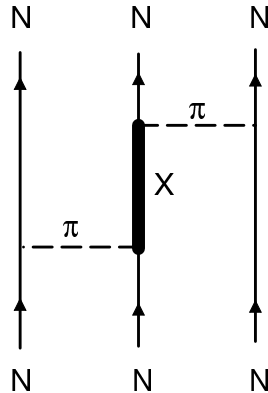


Figure 3.4: Diagrammatic representation of the process providing the main contribution to the three-nucleon interaction. The thick solid line corresponds to an excited state of the nucleon.

The three-nucleon potential is usually written in the form

$$V_{ijk} = V_{ijk}^{2\pi} + V_{ijk}^N, \quad (3.41)$$

where the first contribution takes into account the process of Fig. 3.4 while  $V_{ijk}^N$  is purely phenomenological. The two parameters entering the definition of the three-body potential are adjusted in such a way as to reproduce the properties of  ${}^3H$  and  ${}^3He$ . Note that the



inclusion of  $V_{ijk}$  leads to a very small change of the total potential energy, the ratio  $\langle V_{ijk} \rangle / \langle v_{ij} \rangle$  being  $\sim 2\%$ .

For  $A > 3$  the Schrödinger equation is no longer exactly solvable. The ground state energy of nuclei having  $A \geq 4$  can be estimated from Ritz principle, stating that the expectation value of the hamiltonian in the trial state  $|\Psi_V\rangle$  satisfies

$$E_V = \frac{\langle \Psi_V | H | \Psi_V \rangle}{\langle \Psi_V | \Psi_V \rangle} \geq E_0 , \quad (3.42)$$

$E_0$  being the ground state energy. Obviously, the larger the overlap  $\langle \Psi_0 | \Psi_V \rangle$  the closer  $E_V$  is to  $E_0$ .

In the variational approach based on Eq. (3.42)  $E_0$  is estimated carrying out a functional minimization of  $E_V$ . The trial ground state is written in such a way as to reflect the structure of the nuclear interaction hamiltonian. For few nucleon systems it takes the form

$$|\Psi_V\rangle = (1 + U) |\Psi_P\rangle , \quad (3.43)$$

where

$$|\Psi_P\rangle = F |\Phi_A(JJ_3TT_3)\rangle . \quad (3.44)$$

In the above equations  $|\Phi_A(JJ_3TT_3)\rangle$  is a shell model state, describing  $A$  independent particles coupled to total angular momentum  $J$  and total isospin  $T$ , with third components  $J_3$  and  $T_3$ , while the operators  $U$  and  $F$  take into account the correlation structure induced by the two- and three-nucleon potentials, respectively. The dominant correlation effects, associated with the NN potential  $v_{ij}$ , are described by the operator  $F$ , which is usually written

$$F = \mathcal{S} \prod_{j>i=1}^A f_{ij} , \quad (3.45)$$

where  $\mathcal{S}$  is the symmetrization operator and (compare to Eq. (3.36))

$$f_{ij} = \sum_{n=1}^6 f^{(n)}(r_{ij}) O_{ij}^{(n)} . \quad (3.46)$$

The shape of the radial correlation functions  $f^{(n)}$  are determined by minimizing the expectation value  $E_V$ . In few nucleon systems this procedure is implemented choosing suitable analytical expressions involving few adjustable parameters.

The main features of the  $f^{(n)}$  are dictated by the behaviour of the corresponding component of the potential  $v_{ij}$ . For example, due to the presence of the strong repulsive core  $f^{(n)}(r) \ll 1$  at  $r \lesssim 1$  fm. A typical set of radial correlation functions is shown in Fig. 3.5.

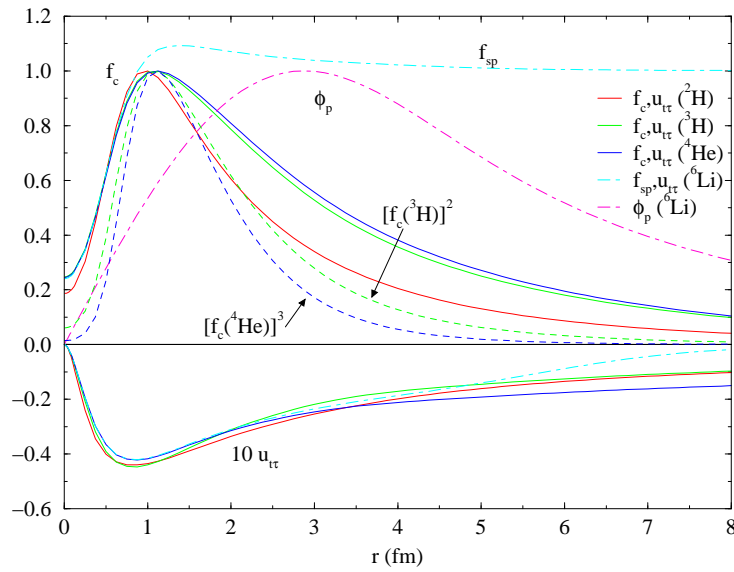


Figure 3.5: Correlation functions in few nucleon systems: the central and tensor-isospin components  $f^{(1)}$  and  $f^{(4)}$  are denoted by  $f_c$  and  $u_{t\tau}$ , respectively. The dashed lines show  $f_c^2(^3\text{H})$  and  $f_c^3(^4\text{He})$  to illustrate the large  $r$  behavior. The dot-dashed line marked  $\phi_p$  shows the independent particle model wave function for  $^6\text{Li}$ .

The main difficulty of the variational approach is the calculation of the expectation value  $E_V$ , involving an integration over  $3A$  space coordinate as well as a sum over the spin-isospin degrees of freedom, which makes the dimensionality of the problem very difficult to handle for  $A \geq 8$ .

To understand this problem, let us write the variational state in the form

$$|\Psi_V\rangle = \sum_n \Psi_n(R) |n\rangle, \quad (3.47)$$

where the sum includes all possible spin-isospin states, labelled by the index  $n$ , and  $R \equiv \{\mathbf{r}_1, \dots, \mathbf{r}_A\}$  specifies the space configuration of the system. For example, in the case of  ${}^3He$  ( $J = T = 1/2$ ) one finds

$$\begin{aligned} |1\rangle &= |\uparrow p \uparrow n \downarrow n\rangle \\ |2\rangle &= |\downarrow p \uparrow n \downarrow n\rangle \\ |3\rangle &= |\downarrow n \uparrow p \downarrow n\rangle \\ \dots &= \dots \end{aligned} \quad (3.48)$$

The possible spin states of  $A$  spin-1/2 particles are  $2^A$  and, since  $Z$  of the  $A$  nucleons can be protons, there are  $A!/Z!(A-Z)!$  isospin states. Hence, the sum over  $n$  in Eq. (3.47) involves

$$M = 2^A \frac{A!}{Z!(A-Z)!} \quad (3.49)$$

contributions.

In the representation of Eq. (3.47) the nuclear hamiltonian  $H$  is a  $M \times M$  matrix whose elements depend upon  $R$ . To obtain  $E_V$  one has to evaluate the  $M \times M$  integrals

$$\int dR \Psi_n^\dagger(R) H_{nm} \Psi_m(R), \quad (3.50)$$

whose calculation is carried out using the Monte Carlo (MC) method.

The expectation value of any operator  $O$  in the state  $\Psi_V$  can be written in the form

$$\begin{aligned} \langle O \rangle &= \sum_{m,n} \int dR \left[ \frac{\Psi_m^\dagger(R) O_{mn}(R) \Psi_n(R)}{P_{mn}(R)} \right] P_{mn}(R) \\ &= \sum_{m,n} \int dR \tilde{O}_{mn}(R) P_{mn}(R), \end{aligned} \quad (3.51)$$

with

$$\tilde{O}_{mn} = \frac{\Psi_m^\dagger(R) O_{mn}(R) \Psi_n(R)}{P_{mn}(R)}, \quad (3.52)$$

the probability distribution  $P_{mn}(\mathbf{R})$  being given by

$$P_{mn}(R) = |\text{Re}(\Psi_m^\dagger(R) \Psi_n(R))|. \quad (3.53)$$

Let  $\{R_p\} \equiv \{R_1, \dots, R_{N_c}\}$  be a set of  $N_c$  configurations drawn from the probability distribution of Eq. (3.51), i.e. such that the probability that a configuration  $\tilde{R}$  belongs to the set  $\{R_p\}$  is proportional to  $P_{mn}(R)$ . It then follows that

$$\int dR \tilde{O}_{mn}(R) P_{mn}(R) = \lim_{N_c \rightarrow \infty} \frac{1}{N_c} \sum_{p=1}^{N_c} \tilde{O}_{mn}(R_p). \quad (3.54)$$

The above procedure, called Variational Monte Carlo (VMC) method, allows one to obtain estimates of the ground state energy  $E_0$  whose accuracy is limited by the statistical error associated with the use of a finite configuration set and by the uncertainty in the choice of the trial wave function. The second source of error can be removed using the Green Function Monte Carlo (GFMC) approach.

Let  $\{|\Psi_m\rangle\}$  be the complete set of eigenstates of the nuclear hamiltonian, satisfying

$$H|\Psi_m\rangle = E_m|\Psi_m\rangle. \quad (3.55)$$

The trial variational wave function can obviously be expanded according to

$$|\Psi_V\rangle = \sum_n \beta_n |\Psi_m\rangle, \quad (3.56)$$

implying

$$\lim_{\tau \rightarrow \infty} e^{-H\tau} |\Psi_V\rangle = \lim_{\tau \rightarrow \infty} \sum_n \beta_n e^{-E_m\tau} |\Psi_m\rangle = \beta_0 e^{-E_0\tau} |\Psi_0\rangle. \quad (3.57)$$

Hence, evolution of the variational ground state to infinite imaginary time projects out the *true* ground state of the nuclear hamiltonian and allows one to extract the corresponding eigenvalue.

The calculation is carried out dividing the imaginary time interval  $\tau$  in  $N$  steps of length  $\Delta\tau = \tau/N$  to rewrite

$$e^{-H\tau} = (e^{-H\Delta\tau})^N . \quad (3.58)$$

The state at imaginary time  $(i+1)\Delta\tau$  is can be obtained from the one corresponding to  $\tau = i\Delta\tau$  through the relation

$$|\Psi_V^{i+1}\rangle = e^{-H\Delta\tau} |\Psi_V^i\rangle , \quad (3.59)$$

that can be rewritten ( $|RST\rangle$  specifies the configuration of the system in coordinate, spin and isospin space)

$$\langle R'S'T' | \Psi_V^{i+1} \rangle = \sum_{ST} \int dR \langle R'S'T' | e^{-H\Delta\tau} | RST \rangle \langle RST | \Psi_V^i \rangle \quad (3.60)$$

or

$$\Psi_{V,S'T'}^{i+1}(R) = \sum_{ST} \int dR' G_{S'T',ST}(R', R) \Psi_{V,ST}^i(R) , \quad (3.61)$$

The Green's function appearing in the above equation, yielding the amplitude for the system to evolve from  $|RST\rangle$  to  $|R'S'T'\rangle$  during the imaginary time interval  $\Delta\tau$ , is defined as

$$G_{S'T',ST}(R', R) = \langle R'S'T' | e^{-H\Delta\tau} | RST \rangle . \quad (3.62)$$

The GFMC approach has been succesfully employed to describe the ground state and the low lying excited states of nuclei having  $A$  up to 8. The results of these calculations, summarized in Table 3.1 and Fig. 3.6, show that the nonrelativistic approach, based on a dynamics modeled to reproduce the properties of two- and three-nucleon systems, has a remarkable predictive power.

### 3.5.2 Nuclear matter

In the case of neutron stars, correponding to  $A \sim 10^{57}$ , the computational techniques described in Section 3.5.1 cannot be applied and approximations need to be made.

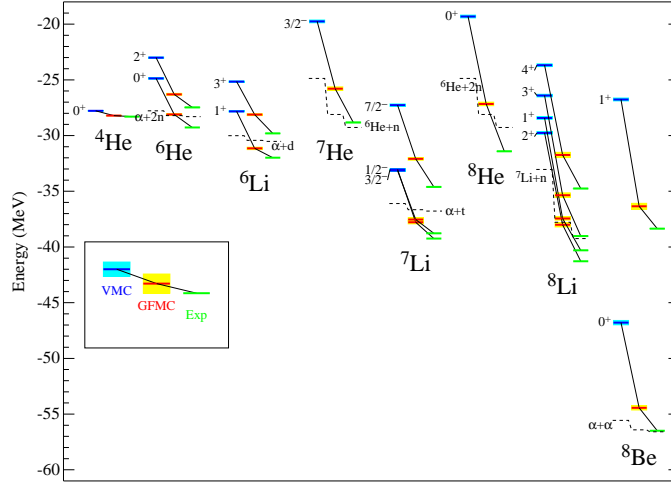


Figure 3.6: VMC and GFMC energies of nuclei with  $A \leq 8$  compared to experiment.

In the simplest scheme the complicated NN potential is replaced by a *mean field*. This amount to substituting

$$\sum_{j>i=1}^A v_{ij} \rightarrow \sum_{i=1}^A U_i, \quad (3.63)$$

in Eq. (3.39), with the potential  $U$  chosen in such a way that the *single particle* hamiltonian

$$h_0 = \frac{p^2}{2m} + U \quad (3.64)$$

be diagonalizable. Within this framework the nuclear ground state wave function reduces to a Slater determinant, constructed using the  $A$  lowest energy eigenstates of  $h_0$ :

$$|\Psi_0\rangle = \frac{1}{\sqrt{A!}} \det\{\phi_i\}, \quad (3.65)$$

the  $\phi_i$ 's ( $i = 1, 2, \dots, A$ ) being solutions of the Schrödinger equation

$$h_0|\phi_i\rangle = \epsilon_i|\phi_i\rangle, \quad (3.66)$$

and the corresponding ground state energy is given by

$$E_0 = \sum_{i=1}^A \epsilon_i. \quad (3.67)$$

${}^AZ(J^\pi; T)$	VMC ( $\Psi_T$ )	VMC ( $\Psi_V$ )	GFMC	Expt
${}^2\text{H}(1^+; 0)$	-2.2248(5)			-2.2246
${}^3\text{H}((1/2)^+; 1/2)$	-8.15(1)	-8.32(1)	-8.47(1)	-8.48
${}^4\text{He}(0^+; 0)$	-26.97(3)	-27.78(3)	-28.34(4)	-28.30
${}^6\text{He}(0^+; 1)$	-23.64(7)	-24.87(7)	-28.11(9)	-29.27
${}^6\text{Li}(1^+; 0)$	-27.10(7)	-27.83(5)	-31.15(11)	-31.99
${}^7\text{He}((3/2)^-; 3/2)$	-18.05(11)	-19.75(12)	-25.79(16)	-28.82
${}^7\text{Li}((3/2)^-; 1/2)$	-31.92(11)	-33.04(7)	-37.78(14)	-39.24
${}^8\text{He}(0^+; 2)$	-17.98(8)	-19.31(12)	-27.16(16)	-31.41
${}^8\text{Li}(2^+; 1)$	-28.00(14)	-29.76(13)	-38.01(19)	-41.28
${}^8\text{Be}(0^+; 0)$	-45.47(16)	-46.79(19)	-54.44(19)	-56.50

Table 3.1: Experimental and quantum Monte Carlo ground state energies of nuclei with  $A=2-8$  in MeV. The columns marked VMC( $\Psi_V$ ) and GFMC show the VMC and GFMC results, respectively.

This procedure is the basis of the nuclear shell model, that has been successfully applied to explain many nuclear properties.

Matter in the neutron star interior, however, is a uniform, dense nuclear fluid, whose single particle wave functions are known to be plane waves, as dictated by translational invariance. Shell effects are not expected to play a major role in such a system. On the other hand, strong correlations between nucleons induced by the NN potential, not taken into account within the mean field approximation, become more and more important as the density increases, and can not be disregarded.

Let us first consider symmetric nuclear matter, defined as a uniform extended system containing equal numbers of proton and neutrons which interact through strong interactions only. Neglecting, for the sake of simplicity, three-nucleon forces, the nuclear matter hamiltonian can be written as in Eq.(3.39) with  $v_{ij}$  denoting the NN potential. In absence

of interactions, the wave function is a Slater determinant of single particle states

$$\varphi_{\mathbf{k}\sigma\tau}(\mathbf{r}) = \frac{1}{\sqrt{V}} e^{i\mathbf{k}\cdot\mathbf{r}} \chi_{\sigma}\eta_{\tau} , \quad (3.68)$$

where  $\chi$  and  $\eta$  are the Pauli spinors describing spin and isospin, respectively, and  $|\mathbf{k}| < k_F = (3\pi^2 n/2)^{1/3}$ ,  $n$  being the matter density.

The main problem associated with the application of many-body perturbation theory to nuclear matter is the presence of the strongly repulsive core in the NN potential (see Section 3.3 and Fig. 3.3), that makes the matrix elements

$$\langle \varphi_{\mathbf{k}_1\sigma_1\tau_1} \varphi_{\mathbf{k}_2\sigma_2\tau_2} | v_{12} | \varphi_{\mathbf{k}_1\sigma_1\tau_1} \varphi_{\mathbf{k}_2\sigma_2\tau_2} \rangle \quad (3.69)$$

very large or even divergent. As we will see, this difficulty can be circumvented either through a proper redefinition of the interaction potential or changing the basis of states describing the “unperturbed” system.

### A. G-matrix perturbation theory

Within the first approach the hamiltonian is first split in two pieces according to

$$H = H_0 + H_1 , \quad (3.70)$$

with

$$H_0 = \sum_{i=1}^N (K_i + U_i) , \quad (3.71)$$

where  $K = -\nabla^2/2m$  is the kinetic energy operator, and

$$H_1 = \sum_{j>i=1}^N v_{ij} - \sum_{i=1}^N U_i , \quad (3.72)$$

with the single particle potential generally chosen in such a way as to make the perturbative expansion rapidly convergent. The interaction hamiltonian  $H_1$  is then treated perturbatively, summing up infinite set of diagrams to overcome the problems associated



with the calculation of the matrix elements (3.69). This procedure leads to the integral equation defining the  $G$ -matrix

$$G(W) = v - v \frac{Q}{W} G . \quad (3.73)$$

The  $G$ -matrix, as diagrammatically illustrated in Fig. 3.7, is the operator describing NN scattering in the nuclear medium. The quantity  $W$  appearing in Eq. (3.73) is the energy denominator associated with the propagator of the intermediate state, while the operator  $Q$  prevents scattering to states in the Fermi sea, forbidden by Pauli exclusion principle.

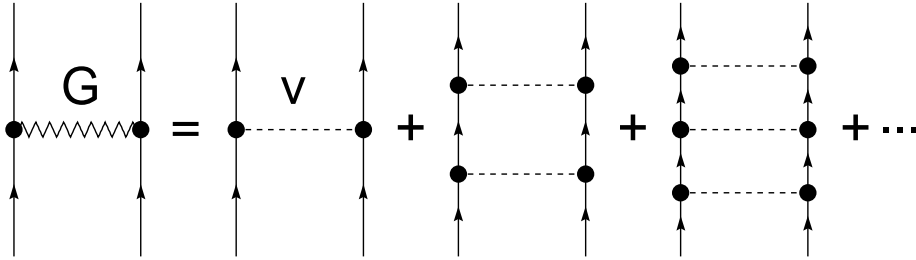


Figure 3.7: Diagrammatic representation of Eq. (3.73).

The state describing two interacting nucleons  $\psi_{ij}$  can be expressed in terms of  $G$  through the Bethe-Goldstone equation

$$\psi_{ij} = \phi_{ij} - \frac{Q}{W} G \psi_{ij} , \quad (3.74)$$

where  $\phi_{ij} = \varphi_i \varphi_j$ , with  $\varphi_i = \varphi_{\mathbf{k}_i \sigma_i \tau_i}$  given by Eq. (3.68), is the corresponding unperturbed state. From Eq. (3.74) it follows that the matrix elements of  $G$  between unperturbed states

$$\langle \phi_{i'j'} | G | \phi_{ij} \rangle = \langle \phi_{i'j'} | v | \psi_{ij} \rangle \quad (3.75)$$

are well behaved.

Although the expansion in powers of  $G$  is still not convergent, the terms in the perturbative series can be grouped in such a way as to obtain a convergent expansion in powers of the quantity

$$\kappa = n \sum_{ij} \int d^3r |\phi_{ij}(r) - \psi_{ij}(r)|^2, \quad (3.76)$$

where the sum is extended to all states belonging to the Fermi sea. The definition shows that  $\kappa$  measures the average distortion of the two-nucleon wave function produced by NN forces.

Nuclear matter calculations carried out within  $G$ -matrix perturbation theory include contributions of order  $\kappa^3$  to the energy per nucleon. The results show that the convergence strongly depends on the choice of the single particle potential  $U$ .

## B. CBF perturbation theory

In the alternative approach, called Correlated Basis Functions (CBF) perturbation theory, the nonperturbative effects arising from the short range repulsive core of the interaction potential are incorporated in the basis functions. The unperturbed Fermi gas states  $|n_0\rangle$  are replaced by the set of correlated states

$$|n\rangle = \frac{F|n_0\rangle}{\langle n_0|F^\dagger F|n_0\rangle^{1/2}}, \quad (3.77)$$

where  $F$  is the *correlation operator*, whose structure reflects the complexity of the NN potential. In most nuclear matter applications  $F$  is written in the form

$$F = \mathcal{S} \prod_{j>i=1}^A f_{ij}, \quad (3.78)$$

where

$$f_{ij} = \sum_n f^{(n)}(r_{ij}) O_{ij}^{(n)}, \quad (3.79)$$

$\mathcal{S}$  is the operator that symmetrizes the product on its right hand side and the operators  $O^{(n)}$  are defined in Eq. (3.38).

The correlated states (3.77) form a complete set but are *not* orthogonal to one another. However, they can be orthogonalized using standard techniques of many-body perturbation theory.

The radial shapes of the  $f^{(n)}(r)$  are determined minimizing the expectation value  $E_V = \langle 0|H|0\rangle$ . In nuclear matter, this procedure leads to a set of Euler-Lagrange equations, whose solutions satisfy the boundary conditions

$$\lim_{r \rightarrow \infty} f^{(n)}(r) = \begin{cases} 1 & n = 1 \\ 0 & n > 1 \end{cases} . \quad (3.80)$$

The short range behaviour of the two-nucleon correlation functions is such that the quantity

$$f_{ij}^\dagger H_{ij} f_{ij} = f_{ij}^\dagger \left( \frac{\mathbf{p}_i^2}{2m} + \frac{\mathbf{p}_j^2}{2m} + v_{ij} \right) f_{ij}, \quad (3.81)$$

which reduces to  $H_{ij}$  at large interparticle distances, is well behaved as  $r \rightarrow 0$ .

Once the correlated basis has been defined, the nuclear hamiltonian can be split in two pieces according to Eq. (3.70), where  $H_0$  and  $H_1$  are now defined as the diagonal and off diagonal part of  $H$  in the correlated basis, respectively. We can then write

$$\langle m|H_0|n\rangle = \delta_{mn} \langle m|H|n\rangle \quad (3.82)$$

$$\langle m|H_1|n\rangle = (1 - \delta_{mn}) \langle m|H|n\rangle . \quad (3.83)$$

If the two-body correlation function has been properly chosen, i.e. if  $E_V$  is close to the eigenvalue  $E_0$ , the correlated states have large overlaps with the true eigenstates of the nuclear hamiltonian and the matrix elements of  $H_1$  are small. Hence, the perturbative expansion in powers of  $H_1$  is expected to be rapidly convergent.

The explicit calculation of matrix elements of  $H$  between correlated states involves prohibitive difficulties, as it requires integrations over the coordinates of a huge number of particles. It is usually performed expanding the matrix element in a series whose terms represent the contributions of subsystems (clusters) containing an increasing number (2, 3,

..., A) of nucleons. The terms in the series can be classified according to their topological structure and summed up to all orders solving a set of coupled integral equations, called Fermi Hyper-Netted Chain (FHNC) equations.

### 3.6 Relativistic mean field theory

The theoretical approach described in the previous section is based on the assumption that the degrees of freedom associated with the carriers of the NN interaction can be eliminated in favor of a static NN potential. While this procedure appears to be most successful at  $\rho \sim \rho_0$ , as matter density (and therefore the nucleon Fermi momentum) increases the relativistic propagation of the nucleons, as well as the retarded propagation of the virtual meson fields giving rise to nuclear forces, are expected to become more and more important.

In principle, relativistic quantum field theory provides a well defined theoretical framework in which relativistic effects can be taken into account in a fully consistent fashion. Due to the complexity and nonperturbative nature of the interaction, however, the *ab initio* approach to the nuclear many problem, based on the QCD lagrangian, involves prohibitive difficulties. In fact, even the structure of individual hadrons, like the proton or the  $\pi$  meson, is not yet understood at a fully quantitative level in terms of QCD degrees of freedom. Let alone the structure of highly condensed hadronic matter at supernuclear densities.

It has to be pointed out, however, that when dealing with condensed matter it is often convenient to replace the lagrangian describing the interactions between elementary constituents, be it solvable or not, with properly constructed *effective interactions*. For example, the properties of highly condensed systems bound by electromagnetic interactions are most successfully explained using effective interatomic potentials. In spite of the fact that the lagrangian of quantum electrodynamics is very well known and can be

treated in perturbation theory, nobody in his right mind would ever use it to carry out explicit calculations in condensed matter physics.

The fact that most of the time nucleons in nuclear matter behave as individual particles interacting through boson exchange, suggests that the fundamental degrees of freedom of QCD, quarks and gluons, may indeed be replaced by nucleons and mesons, to be regarded as the degrees of freedom of an *effective* field theory.

In this section we will describe a simple model in which nuclear matter is viewed as a static uniform system of nucleons, described by Dirac spinors, interacting through exchange of a scalar and a vector meson, called  $\sigma$  and  $\omega$ , respectively.

The basic ingredient of the  $\sigma$ - $\omega$  model is the lagrangian density

$$\mathcal{L} = \mathcal{L}_N + \mathcal{L}_B + \mathcal{L}_{int} , \quad (3.84)$$

where  $\mathcal{L}_N$ ,  $\mathcal{L}_B$  and  $\mathcal{L}_{int}$  describe free nucleons and mesons and their interactions, respectively. The dynamics of the free nucleon field is dictated by the Dirac lagrangian of Eq. (3.24)

$$\mathcal{L}_N(x) = \bar{\psi}(x) (i\rlap{/}\partial - m) \psi(x) , \quad (3.85)$$

where the nucleon field, denoted by  $\psi(x)$ , combines the two four-component Dirac spinors describing proton and neutron, as in Eq. (3.25). The meson lagrangian reads

$$\begin{aligned} \mathcal{L}_B(x) &= \mathcal{L}_\omega(x) + \mathcal{L}_\sigma(x) \\ &= -\frac{1}{4}F^{\mu\nu}(x)F_{\mu\nu}(x) + \frac{1}{2}m_\omega^2 V_\mu(x)V^\mu(x) \\ &+ \frac{1}{2}\partial_\mu\phi(x)\partial^\mu\phi(x) - \frac{1}{2}m_\sigma^2\phi(x)^2 \end{aligned} \quad (3.86)$$

where

$$F_{\mu\nu}(x) = \partial_\nu V_\mu(x) - \partial_\mu V_\nu(x) , \quad (3.87)$$

$V_\mu(x)$  and  $\sigma(x)$  are the vector and scalar meson fields, respectively, and  $m_\omega$  and  $m_\sigma$  the corresponding masses.

In specifying the form of the interaction lagrangian we will require that, besides being a Lorentz scalar,  $\mathcal{L}_{int}(x)$  gives rise to a Yukawa-like meson exchange potential in the static limit. Hence, we write

$$\mathcal{L}_{int}(x) = g_\sigma \phi(x) \bar{\psi}(x) \psi(x) - g_\omega V_\mu(x) \bar{\psi}(x) \gamma^\mu \psi(x) , \quad (3.88)$$

where  $g_\sigma$  and  $g_\omega$  are coupling constants and the choice of signs reflect the fact that the NN interaction contains both attractive and repulsive contributions.

The equations of motion for the fields follow from the Euler-Lagrange equations associated with the lagrangian density of Eq. (3.84). The meson fields satisfy

$$(\square + m_\sigma^2) \phi(x) = g_\sigma \bar{\psi}(x) \psi(x) \quad (3.89)$$

and

$$(\square + m_\omega^2) V_\mu(x) - \partial_\mu(\partial^\nu V_\nu) = g_\omega \bar{\psi}(x) \gamma_\mu \psi(x) , \quad (3.90)$$

while the evolution of the nucleon field is dictated by the equation

$$[(\not{\partial} - g_\omega \gamma_\mu V^\mu(x)) - (m - g_\sigma \phi(x))] \psi(x) = 0 . \quad (3.91)$$

The above coupled equations are fully relativistic and Lorentz covariant. However, their solution involves prohibitive difficulties. Here we will restrict ourselves to the discussion of an approximation scheme widely used to solve Eqs. (3.89)-(3.91), known as *mean field* approximation, that essentially amounts to treat  $\phi(x)$  and  $V_\mu(x)$  as classical fields.

We replace the meson field with their mean values in the ground state of static and uniform nuclear matter

$$\phi(x) \rightarrow \langle \phi(x) \rangle , \quad V_\mu(x) \rightarrow \langle V_\mu(x) \rangle , \quad (3.92)$$

where  $\langle \phi(x) \rangle$  and  $\langle V_\mu(x) \rangle$  must be computed from the equations of motion. In static and uniform nuclear matter the baryon and scalar densities,  $n_B = \psi^\dagger \psi$  and  $n_s = \bar{\psi} \psi$ , as well

as the current  $j_\mu = \bar{\psi}\gamma_\mu\psi$ , are constants, independent of  $x$ . As a consequence, the mean values of the meson fields are also constants satisfying the relations

$$m_\sigma^2 \langle \phi \rangle = g_\sigma \langle \bar{\psi}\psi \rangle \quad (3.93)$$

$$m_\omega^2 \langle V_0 \rangle = g_\omega \langle \psi^\dagger\psi \rangle \quad (3.94)$$

$$m_\omega^2 \langle V_i \rangle = g_\omega \langle \bar{\psi}\gamma_i\psi \rangle, \quad i = 1, 2, 3. \quad (3.95)$$

The nucleon equation of motion, rewritten in terms of the mean values of the meson fields, reads

$$[(\not{\partial} - g_\omega\gamma_\mu\langle V^\mu \rangle) - (m - g_\sigma\langle \phi \rangle)]\psi(x) = 0. \quad (3.96)$$

In static and uniform matter, the nucleon states must be eigenstates of the four-momentum operator, that can be written as

$$\psi_{\mathbf{k}}e^{ikx} = \psi_{\mathbf{k}}e^{ik_\mu x^\mu} = \psi_{\mathbf{k}}e^{i(k_0t - \mathbf{k}\cdot\mathbf{r})}, \quad (3.97)$$

the  $\psi_{\mathbf{k}}$  being solutions of

$$\begin{aligned} & [(\not{k} - g_\omega\gamma_\mu\langle V^\mu \rangle) - (m - g_\sigma\langle \phi \rangle)]\psi_{\mathbf{k}} \\ & = [\gamma_\mu(k^\mu - g_\omega\langle V^\mu \rangle) - (m - g_\sigma\langle \phi \rangle)]\psi_{\mathbf{k}} = 0. \end{aligned} \quad (3.98)$$

The above equation can be recast in a form reminiscent of the Dirac equation. Defining

$$K_\mu = k_\mu - g_\omega\langle V^\mu \rangle \quad (3.99)$$

$$m^* = m - g_\sigma\langle \phi \rangle, \quad (3.100)$$

we obtain

$$(\not{K} - m^*)\psi_{\mathbf{k}} = 0. \quad (3.101)$$

The corresponding energy eigenvalues can be found from

$$\begin{aligned}
(\not{K} + m^*)(\not{K} - m^*) &= \not{K}\not{K} - m^{*2} = K_\mu K_\nu \gamma^\mu \gamma^\nu - m^{*2} \\
&= K_\mu K_\nu \frac{\gamma^\mu \gamma^\nu + \gamma^\nu \gamma^\mu}{2} - m^{*2} \\
&= K_\mu K^\mu - m^{*2} ,
\end{aligned} \tag{3.102}$$

implying

$$(K_\mu K^\mu - m^{*2}) \psi_{\mathbf{k}} = 0 , \tag{3.103}$$

leading to

$$(K_\mu K^\mu - m^{*2}) = 0 \tag{3.104}$$

and

$$\begin{aligned}
K_0 &= E_{\mathbf{k}} = k_0 - g_\omega \langle V_0 \rangle = \sqrt{|\mathbf{K}|^2 + m^{*2}} \\
&= \sqrt{|\mathbf{k} - g_\omega \langle \mathbf{V} \rangle|^2 + (m - g_\sigma \langle \phi \rangle)^2} .
\end{aligned} \tag{3.105}$$

It follows that the energy eigenvalues associated with nucleons and antinucleons can be written

$$e_{\mathbf{k}} = E_{\mathbf{k}} + g_\omega \langle V_0 \rangle \tag{3.106}$$

and

$$\bar{e}_{\mathbf{k}} = E_{\mathbf{k}} - g_\omega \langle V_0 \rangle , \tag{3.107}$$

respectively. The above equations give the nucleon (and antinucleon) energies in terms of the mean values of the meson fields, which are in turn defined in terms of the ground state expectation values of the nucleon densities and current, according to Eqs. (3.93)-(3.95).

The ground state expectation value of an operator  $\bar{\psi}\Gamma\psi$  can be evaluated exploiting the fact that each nucleon state is specified by its momentum,  $\mathbf{k}$ , and spin-isospin projections. Denoting the average of  $\bar{\psi}\Gamma\psi$  in a single particle state by  $\langle \bar{\psi}\Gamma\psi \rangle_{\mathbf{k}\alpha}$ , where the index  $\alpha$



labels the spin-isospin state, we can write the ground state expectation value as

$$\langle \bar{\psi} \Gamma \psi \rangle = \sum_{\alpha} \int \frac{d^3 k}{(2\pi)^3} \langle \bar{\psi} \Gamma \psi \rangle_{\mathbf{k}\alpha} \theta(e_F - e_{\mathbf{k}}) , \quad (3.108)$$

where the  $\theta$ -function restricts the momentum integration to the region corresponding to energies lower than the Fermi energy  $e_F$ . To obtain the single particle average  $\langle \bar{\psi} \gamma_{\mu} \psi \rangle_{\mathbf{k}\alpha}$ , we use Eq. (3.101), implying

$$k_0 = \gamma_0 (\boldsymbol{\gamma} \cdot \mathbf{k} + g_{\omega} \gamma_{\mu} \langle V^{\mu} \rangle + m^*) . \quad (3.109)$$

The quantity defined by the above equation can be regarded as the single nucleon hamiltonian, whose eigenvalues are given by (compare to Eq. (3.106))

$$\langle k_0 \rangle_{\mathbf{k}\alpha} = \langle \psi^{\dagger} k_0 \psi \rangle_{\mathbf{k}\alpha} = E_{\mathbf{k}} + g_{\omega} \langle V_0 \rangle . \quad (3.110)$$

The ground state expectation value of the baryon density can be readily evaluated from Eqs. (3.109) and (3.110) noting that

$$\begin{aligned} \frac{\partial}{\partial \langle V_0 \rangle} \langle \psi^{\dagger} k_0 \psi \rangle_{\mathbf{k}\alpha} &= \frac{\partial}{\partial \langle V_0 \rangle} (E_{\mathbf{k}} + g_{\omega} \langle V_0 \rangle) = g_{\omega} \\ &= \langle \psi^{\dagger} \frac{\partial k_0}{\partial \langle V_0 \rangle} \psi \rangle_{\mathbf{k}\alpha} = g_{\omega} \langle \psi^{\dagger} \psi \rangle_{\mathbf{k}\alpha} , \end{aligned} \quad (3.111)$$

implying

$$\langle \psi^{\dagger} \psi \rangle_{\mathbf{k}\alpha} = 1 . \quad (3.112)$$

It follows that  $n_B$  can be obtained using Eq. (3.108), leading to

$$n_B = \langle \psi^{\dagger} \psi \rangle = \nu \int \frac{d^3 k}{(2\pi)^3} \theta(e_F - e_{\mathbf{k}}) , \quad (3.113)$$

where  $\nu$  is the degeneracy of the momentum eigenstate ( $\nu = 2$  and  $4$  for pure neutron matter and symmetric nuclear matter, respectively).

The same procedure can be applied to calculate the ground state expectation value  $\langle \bar{\psi} \gamma^i \psi \rangle$  ( $i = 1, 2, 3$ ). Taking the derivative with respect to  $k_i$  we find

$$\begin{aligned} \frac{\partial}{\partial k_i} \langle \psi^\dagger k_0 \psi \rangle_{\mathbf{k}\alpha} &= \frac{\partial}{\partial k_i} (E_{\mathbf{k}} + g_\omega \langle V_0 \rangle) = \frac{\partial E_{\mathbf{k}}}{\partial k_i} \\ &= \langle \psi^\dagger \frac{\partial k_0}{\partial k_i} \psi \rangle_{\mathbf{k}\alpha} = \gamma^0 \langle \psi^\dagger \gamma^i \psi \rangle_{\mathbf{k}\alpha} = \langle \bar{\psi} \gamma^i \psi \rangle_{\mathbf{k}\alpha} , \end{aligned} \quad (3.114)$$

leading to

$$\begin{aligned} \langle \bar{\psi} \gamma^i \psi \rangle &= \nu \int \frac{d^3 k}{(2\pi)^3} \left( \frac{\partial E_{\mathbf{k}}}{\partial k_i} \right) \theta(e_F - e_{\mathbf{k}}) \\ &= \nu \int \frac{dk_j dk_k}{(2\pi)^3} \int dE_{\mathbf{k}} \theta(e_F - e_{\mathbf{k}}) = 0 . \end{aligned} \quad (3.115)$$

The above result follows from the fact that, by definition,  $e_{\mathbf{k}} \equiv e_F - g_\omega \langle V_0 \rangle$  everywhere on the boundary of the integration region. The vanishing of the baryon current, that could have been anticipated, as we are dealing with uniform matter in its ground state, implies that the mean values of the space components of the vector field also vanish, i.e. that  $\langle V_i \rangle = 0$ . As a consequence, the energy eigenvalues depend upon the magnitude of the nucleon momentum only, according to

$$e_{\mathbf{k}} = e_k = \sqrt{|\mathbf{k}|^2 + (m - g_\sigma \langle \phi \rangle)^2} + g_\omega \langle V_0 \rangle , \quad (3.116)$$

and the occupied region of momentum space is sphere. Eq. (3.113) then shows that in symmetric nuclear matter, with  $Z=(A-Z)=A/2$ , the baryon density takes the familiar form  $n_B = 2k_F^3/(3\pi^2)$ ,  $k_F$  being the Fermi momentum.

Finally, the scalar density  $n_s = \langle \bar{\psi} \psi \rangle$  can be evaluated from the derivative of  $\langle \psi^\dagger k_0 \psi \rangle_{\mathbf{k}\alpha}$  with respect to  $m$ :

$$\frac{\partial}{\partial m} \langle \psi^\dagger k_0 \psi \rangle_{\mathbf{k}\alpha} = \frac{\partial e_{\mathbf{k}}}{\partial m} = \langle \psi^\dagger \frac{\partial k_0}{\partial m} \psi \rangle_{\mathbf{k}\alpha} = \langle \psi^\dagger \gamma_0 \psi \rangle_{\mathbf{k}\alpha} = \langle \bar{\psi} \psi \rangle_{\mathbf{k}\alpha} , \quad (3.117)$$

yielding

$$\langle \bar{\psi} \psi \rangle_{\mathbf{k}\alpha} = \frac{(m - g_\sigma \langle \phi \rangle)}{\sqrt{|\mathbf{k}|^2 + (m - g_\sigma \langle \phi \rangle)^2}} \quad (3.118)$$

and

$$\langle \bar{\psi} \psi \rangle = \frac{\nu}{2\pi^2} \int_0^{k_F} k^2 dk \frac{(m - g_\sigma \langle \phi \rangle)}{\sqrt{|\mathbf{k}|^2 + (m - g_\sigma \langle \phi \rangle)^2}} \quad (3.119)$$

Collecting together the results of Eqs. (3.113), (3.115) and (3.119) we can rewrite the equations of motion (3.89)-(3.91) in the form:

$$g_\sigma \langle \phi \rangle = \left( \frac{g_\sigma}{m_\sigma} \right)^2 \frac{\nu}{2\pi^2} \int_0^{k_F} |\mathbf{k}|^2 d|\mathbf{k}| \frac{(m - g_\sigma \langle \phi \rangle)}{\sqrt{|\mathbf{k}|^2 + (m - g_\sigma \langle \phi \rangle)^2}} \quad (3.120)$$

$$g_\omega \langle V_0 \rangle = \left( \frac{g_\omega}{m_\omega} \right)^2 \nu \frac{k_F^3}{6\pi^2} \quad (3.121)$$

$$m_\omega^2 \langle V_i \rangle = 0, \quad i = 1, 2, 3. \quad (3.122)$$

Note that, while Eqs. (3.121) and (3.122) are trivial, Eq. (3.120) implies a self-consistency requirement on the mean value of the scalar field, whose value has to satisfy a transcendental equation.

To obtain the equation of state, i.e. the relation between pressure and density (or energy density) of matter, in quantum field theory we start from the energy-momentum tensor, that for a generic Lagrangian  $\mathcal{L} = \mathcal{L}(\phi, \partial_\mu \phi)$  can be written

$$T^{\mu\nu} = \frac{\partial \mathcal{L}}{\partial(\partial_\mu \phi)} \partial^\nu \phi - g^{\mu\nu} \mathcal{L}, \quad (3.123)$$

$g^{\mu\nu}$  being the metric tensor.

In a uniform system the expectation value of  $T^{\mu\nu}$ , is directly related to the energy density,  $\epsilon$ , and pressure,  $P$ , through

$$\langle T_{\mu\nu} \rangle = u_\mu u_\nu (\epsilon + P) - g_{\mu\nu} P, \quad (3.124)$$

where  $u$  denotes the four velocity of the system, satisfying  $u_\mu u^\mu = 1$ . It follows that in the reference frame in which matter is at rest  $\langle T_{\mu\nu} \rangle$  is diagonal and

$$\epsilon = \langle T_{00} \rangle = -\langle \mathcal{L} \rangle + \langle \bar{\psi} \gamma_0 k_0 \psi \rangle \quad (3.125)$$

$$P = \frac{1}{3}\langle T_{ii} \rangle = \langle \mathcal{L} \rangle + \frac{1}{3}\langle \bar{\psi}\gamma_i k_i \psi \rangle. \quad (3.126)$$

Within the mean field approximation, the lagrangian density of the  $\sigma$ - $\omega$  model reduces to

$$\mathcal{L}_{MF} = \bar{\psi} [i\cancel{\partial} - g_\omega \gamma^0 \langle V_0 \rangle - (m - g_\sigma \langle \phi \rangle)] \psi - \frac{1}{2} m_\sigma^2 \langle \phi \rangle^2 + \frac{1}{2} m_\omega^2 \langle V_0 \rangle^2, \quad (3.127)$$

implying

$$T_{MF}^{\mu\nu} = i\bar{\psi}\gamma^\mu \partial^\nu \psi - g^{\mu\nu} \left[ -\frac{1}{2} m_\sigma^2 \langle \phi \rangle^2 - \frac{1}{2} m_\omega^2 \langle V_0 \rangle^2 \right]. \quad (3.128)$$

As a consequence, Eqs. (3.125) and (3.126) become

$$\epsilon = -\langle \mathcal{L}_{MF} \rangle + \langle \bar{\psi}\gamma_0 k_0 \psi \rangle \quad (3.129)$$

$$P = \langle \mathcal{L}_{MF} \rangle + \frac{1}{3}\langle \bar{\psi}\gamma_i k_i \psi \rangle, \quad (3.130)$$

where (use Eqs. (3.110), (3.116) and (3.121))

$$\begin{aligned} \langle \bar{\psi}\gamma_0 k_0 \psi \rangle &= \frac{\nu}{2\pi^2} \int_0^{k_F} |\mathbf{k}|^2 d|\mathbf{k}| \left[ \sqrt{|\mathbf{k}|^2 + (m - g_\sigma \langle \phi \rangle)^2} + g_\omega \langle V_0 \rangle \right] \\ &= g_\omega \langle V_0 \rangle n_B + \frac{\nu}{2\pi^2} \int_0^{k_F} |\mathbf{k}|^2 d|\mathbf{k}| \sqrt{|\mathbf{k}|^2 + (m - g_\sigma \langle \phi \rangle)^2} \\ &= \frac{g_\omega^2}{m_\omega^2} n_B^2 + \frac{\nu}{2\pi^2} \int_0^{k_F} |\mathbf{k}|^2 d|\mathbf{k}| \sqrt{|\mathbf{k}|^2 + (m - g_\sigma \langle \phi \rangle)^2}, \end{aligned} \quad (3.131)$$

and (use eq.(3.115))

$$\langle \bar{\psi}\gamma_i k_i \psi \rangle = \langle \bar{\psi}(\boldsymbol{\gamma} \cdot \mathbf{k})\psi \rangle = \frac{\nu}{2\pi^2} \int_0^{k_F} d|\mathbf{k}| \frac{|\mathbf{k}|^4}{\sqrt{|\mathbf{k}|^2 + (m - g_\sigma \langle \phi \rangle)^2}}. \quad (3.132)$$

Substitution of the above equations into Eqs. (3.129)-(3.130) finally yields (use Eq. (3.127) and the equation of motion for the nucleon field)

$$\epsilon = \frac{1}{2} \frac{m_\sigma^2}{g_\sigma^2} (m - m^*)^2 + \frac{1}{2} \frac{g_\omega^2}{m_\omega^2} n_B^2 + \frac{\nu}{2\pi^2} \int_0^{k_F} |\mathbf{k}|^2 d|\mathbf{k}| \sqrt{|\mathbf{k}|^2 + m^{*2}} \quad (3.133)$$

$$P = -\frac{1}{2} \frac{m_\sigma^2}{g_\sigma^2} (m - m^*)^2 + \frac{1}{2} \frac{g_\omega^2}{m_\omega^2} n_B^2 + \frac{1}{3} \frac{\nu}{2\pi^2} \int_0^{k_F} d|\mathbf{k}| \frac{|\mathbf{k}|^4}{\sqrt{|\mathbf{k}|^2 + m^{*2}}} \quad (3.134)$$

The first two contributions to the right hand side of the above equations arise from the mass terms associated with the vector and scalar fields, while the remaining term gives the energy density and pressure of a relativistic Fermi gas of nucleons of mass  $m^*$  given by (see Eq. (3.120))

$$\begin{aligned} m^* &= m - \frac{g_\sigma^2}{m_\sigma^2} \frac{\nu}{2\pi^2} \int_0^{k_F} |\mathbf{k}|^2 d|\mathbf{k}| \frac{m^*}{\sqrt{|\mathbf{k}|^2 + m^{*2}}} \\ &= m - \frac{g_\sigma^2}{m_\sigma^2} \frac{m^*}{\pi^2} \left[ k_F e_F^* - m^{*2} \ln \left( \frac{k_F + e_F^*}{m^*} \right) \right], \end{aligned} \quad (3.135)$$

with  $e_F^* = \sqrt{k_F^2 + m^{*2}}$ . Equations (3.133)-(3.135) yield energy density and pressure of nuclear matter as a function of the baryon number density  $n_B$  (recall:  $k_F = (6\pi^2 n_B/\nu)^{(1/3)}$ ). The values of the unknown coefficients  $(m_\sigma^2/g_\sigma^2)$  and  $(m_\omega^2/g_\omega^2)$  can be determined by a fit to the empirical saturation properties of nuclear matter, i.e. requiring

$$\frac{B}{A} = \frac{\epsilon(n_0)}{n_0} - m = -16 \text{ MeV} \quad (3.136)$$

with  $n_0 = .16 \text{ fm}^{-3}$ . This procedure leads to the result

$$\frac{g_\sigma^2}{m_\sigma^2} m^2 = 267.1 \quad , \quad \frac{g_\omega^2}{m_\omega^2} m^2 = 195.9 . \quad (3.137)$$

Fig. 3.8 shows the binding energies of symmetric nuclear matter (solid line) and pure neutron matter (dashed line) predicted by the  $\sigma - \omega$  model, plotted against the Fermi momentum  $k_F$ . Note that pure neutron matter is always unbound.

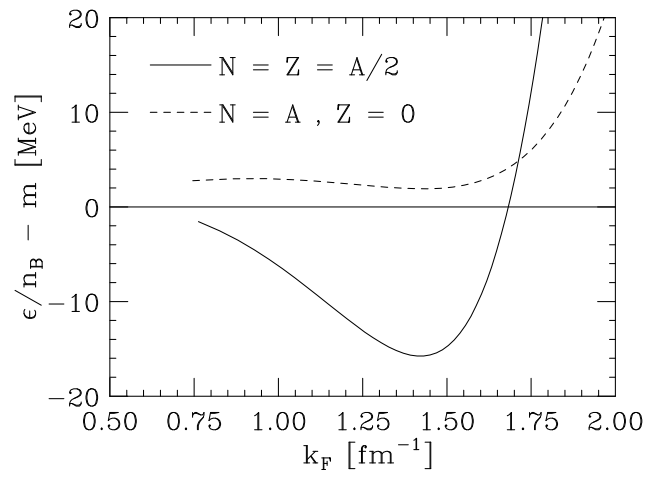


Figure 3.8: Fermi momentum dependence of the binding energy per nucleon of symmetric nuclear matter (solid line) and pure neutron matter (dashed line) evaluated using the  $\sigma - \omega$  model and the mean field approximation.